Nonenzymatic domains of Kalirin7 contribute to spine morphogenesis through interactions with phosphoinositides and Abl

Xin-Ming Ma[a,*], Megan B. Miller[a,*], K. S. Vishwanatha[a], Maegan J. Gross[a], Yanping Wang[a], Thomas Abbott[b], TuKiet T. Lam[b], Richard E. Mains[a], and Betty A. Eipper[a]
[a]Department of Neuroscience, University of Connecticut Health Center, Farmington, CT 06030; [b]WM Keck Foundation Biotechnology Resource Laboratory, Yale/NIDA Neuroproteomics Center, Yale University, New Haven, CT 06511

ABSTRACT **Like several Rho GDP/GTP exchange factors (GEFs), Kalirin7 (Kal7) contains an N-terminal Sec14 domain and multiple spectrin repeats. A natural splice variant of *Kalrn* lacking the Sec14 domain and four spectrin repeats is unable to increase spine formation; our goal was to understand the function of the Sec14 and spectrin repeat domains. Kal7 lacking its Sec14 domain still increased spine formation, but the spines were short. Strikingly, Kal7 truncation mutants containing only the Sec14 domain and several spectrin repeats increased spine formation. The Sec14 domain bound phosphoinositides, a minor but crucial component of cellular membranes, and binding was increased by a phosphomimetic mutation. Expression of KalSec14-GFP in nonneuronal cells impaired receptor-mediated endocytosis, linking Kal7 to membrane trafficking. Consistent with genetic studies placing *Abl*, a non–receptor tyrosine kinase, and the *Drosophila* orthologue of *Kalrn* into the same signaling pathway, Abl1 phosphorylated two sites in the fourth spectrin repeat of Kalirin, increasing its sensitivity to calpain-mediated degradation. Treating cortical neurons of the wild-type mouse, but not the Kal7^{KO} mouse, with an Abl inhibitor caused an increase in linear spine density. Phosphorylation of multiple sites in the N-terminal Sec14/spectrin region of Kal7 may allow coordination of the many signaling pathways contributing to spine morphogenesis.**

Monitoring Editor
Benjamin Margolis
University of Michigan
Medical School

Received: Apr 24, 2013
Revised: Feb 10, 2014
Accepted: Feb 26, 2014

INTRODUCTION

Genetic linkage studies identified *KALRN* as a risk factor for schizophrenia, attention deficit hyperactivity disorder, early-onset coronary artery disease, and stroke (Wang *et al.*, 2007; Lesch *et al.*, 2008; Krug *et al.*, 2010; Kushima *et al.*, 2012). Kalirin7 (Kal7), a Rho GDP/GTP exchange factor (RhoGEF) for Rac1 and RhoG, is the most abundant isoform of the *Kalrn* gene in the adult brain and is localized to the postsynaptic side of excitatory synapses (Ma *et al.*, 2011). Knockout and overexpression studies revealed important roles for Kal7 in dendritic spine formation and synaptic function (Ma *et al.*, 2003, 2008a, 2011; Penzes *et al.*, 2003; Xie *et al.*, 2008; Lemtiri-Chlieh *et al.*, 2011; Cahill *et al.*, 2012), and *KALRN* was implicated in neurological disorders associated with aberrant dendritic spine density and morphology (Youn *et al.*, 2007; Murray *et al.*, 2012).

Although the GEF domain and class 1 PSD-95, discs-large, ZO-1 (PDZ)–binding motif are identical in Kal7 and ΔKal7, a natural splice variant (Figure 1A), the full-length protein is essential for dendritic spine formation (Schiller *et al.*, 2008). Because Kal7 includes a Sec14 domain and four spectrin repeats (SRs) absent from ΔKal7 (Figure 1A), the aim of this study is to determine how these nonenzymatic domains contribute to spine formation. *TRIO* shares the same overall architecture as *KALRN* (Debant *et al.*, 1996), as do *Drosophila trio* and *Caenorhabditis elegans unc-73*, paralogues of *KALRN* and *TRIO* (Figure 1B; McPherson *et al.*, 2005; van Rijssel and van Buul, 2012). Three other RhoGEFs, *Mcf2*, *Mcf2l*, and Purkinje cell atrophy–associated protein-1 (*Puratrophin-1*; *Plekhg4*), also include a Sec14 domain (Figure 1C; (Ueda *et al.*, 2004; Ishikawa *et al.*, 2005; Kostenko *et al.*, 2005). Natural splice variants of *Mcf2* and *Mcf2l* lack the Sec14 domain, as is the case for the ΔKal7 isoform of *Kalrn*.

This article was published online ahead of print in MBoC in Press (http://www.molbiolcell.org/cgi/doi/10.1091/mbc.E13-04-0215) on March 5, 2014.

*These are to be considered equal first authors.

Address correspondence to: Betty Eipper (eipper@uchc.edu), Xin-Ming Ma (ma@uchc.edu).

Abbreviations used: GEF, GDP/GTP exchange factor; Kal7, protein encoded by 7-kb transcript of *Kalrn*; PDZ, PSD-95, discs-large, ZO-1; SR, spectrin repeat.

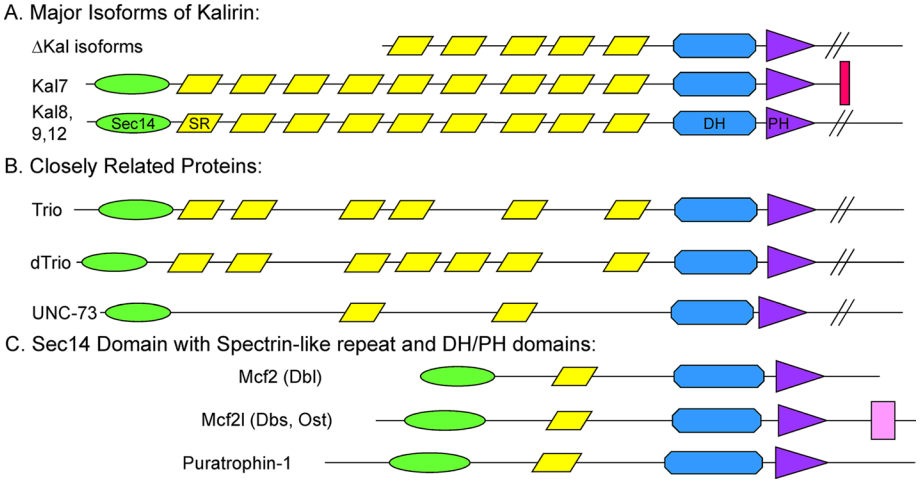

FIGURE 1: RhoGEFs encoded by the *Mus musculus* genome with putative Sec14 and spectrin repeat domains. The N-terminal region of each protein is drawn approximately to scale. (A) Major isoforms of mouse *Kalrn*. The presence of nine spectrin repeats (SRs) was experimentally verified (Vishwanatha *et al.*, 2012). The longer isoforms (Kal8, Kal9, Kal12) contain additional domains (SH3, GEF2, kinase). (B) The N-terminal region of a single splice variant of *Trio* and the *Kalrn/Trio* orthologue in *C. elegans* and *Drosophila melanogaster* is shown with predicted SRs. (C) A single splice variant of each additional *M. musculus* RhoGEF with a predicted Sec14 domain is shown. Sec14, CRAL_TRIO domain, green oval; SR, spectrin-like repeat, yellow parallelogram; DH, Dbl homology domain, blue polygon; PH, pleckstrin homology domain, purple triangle; SH, Src homology 3 domain, pink rectangle; PDZ-binding motif, red bar. *Kalrn*, A2CG49; *Trio*, Q0KL02; *Drosophila trio A*, Q7KVD1; *unc-73A*, O61528; *Mcf2*, A2AEU1; *Mcf2l*, Q64096; *Puratrophin-1* (*Plekhg4*), mFLJ00068.

Yeast Sec14p, the founding member of this family, binds phosphatidylinositol and phosphatidylcholine, mediating their transfer between membranes and coordinating Golgi complex lipid metabolism and protein transport (Mousley *et al.*, 2006; Saito *et al.*, 2007; Schaaf *et al.*, 2008). The Sec14 domains of Mcf2 and Mcf2l play a role in protein localization and regulation of GEF activity (Ueda *et al.*, 2004).

The nine spectrin repeats of Kal7 form nested structures, giving this region an extended, rod-like structure (Vishwanatha *et al.*, 2012); many of the proteins that interact with Kalirin do so by binding to this region (Alam *et al.*, 1996; Colomer *et al.*, 1997; Ratovitski *et al.*, 1999; Koo *et al.*, 2007; Hayashi-Takagi *et al.*, 2010). At least one spectrin-like domain is predicted in the region between the Sec14 and GEF domains of Mcf2 and Mcf2l (Figure 1C). The multiple tandem spectrin repeats of erythrocyte spectrin and skeletal muscle dystrophin provide essential mechanical support and flexibility to the overlying plasma membrane (Giorgi *et al.*, 2006; Sheetz *et al.*, 2006; Ipsaro and Mondragon, 2010). In neurons, controlled calpain-mediated proteolysis of αII-spectrin contributes to dendritic outgrowth and synaptic remodeling (Nicolas *et al.*, 2002; Siminovic *et al.*, 2006; Zadran *et al.*, 2009). Phosphorylation of a single Tyr in αII-spectrin alters its function by decreasing its sensitivity to proteolytic cleavage by μ-calpain (Nicolas *et al.*, 2002; Nedrelow *et al.*, 2003).

Kal7 acts downstream of multiple receptors, including ionotropic receptors (*N*-methyl-D-aspartate [NMDA] receptors), receptor tyrosine kinases (EphB2, ErbB, and platelet-derived growth factor β [PDGFβ]), and G protein–coupled receptors (endothelin receptor and serotonin 2a [$5HT_{2a}$] receptor; Penzes *et al.*, 2003; Jones *et al.*, 2009; Cahill *et al.*, 2012; Wu *et al.*, 2013). Consistent with its role in multiple spine morphogenesis pathways, Kal7 isolated from rat brain is extensively phosphorylated (Kiraly *et al.*, 2011). Threonine 79, situated near the putative lipid-binding pocket of the Kalirin Sec14 domain, can be phosphorylated by CaMKII, protein kinase A, and protein kinase C and is phosphorylated in vivo (Kiraly *et al.*, 2011). Several phosphorylation sites were identified within the first four spectrin repeats of Kalirin, and Fyn, a non–receptor tyrosine kinase, was shown to phosphorylate Tyr-591 in spectrin repeat 4 in vitro (Kiraly *et al.*, 2011). Although axon guidance studies placed *Abl*, another non–receptor tyrosine kinase, and the *Drosophila* orthologue of *Kalrn* into the same pathway (Bateman *et al.*, 2000; Liebl *et al.*, 2000), the underlying mechanism has not been elucidated. Using primary neuronal cultures and examining the properties of the Sec14 and spectrin repeat regions of Kal7, we sought to determine the roles of these noncatalytic domains in controlling the ability of Kal7 to stimulate spine formation and affect spine morphology.

RESULTS

Kal7 and ΔKal7 differ in their effects on spine density, spine length, and synapse formation

Although ΔKal7 and Kal7 are equally active RhoGEFs and have identical PDZ-binding motifs, exogenous Kal7 expressed in cultured cortical neurons localizes to spine-like dendritic protrusions, whereas ΔKal7 localizes more diffusely, with less staining apparent in spines (Schiller *et al.*, 2008). Levels of Kal7 protein are much greater than levels of ΔKal7 in mouse and rat cortex (McPherson *et al.*, 2002; Ma *et al.*, 2008a; Mains *et al.*, 2011; Mandela *et al.*, 2012) and hippocampus (Ma *et al.*, 2008a), and neither protein shows any tendency to oligomerize (Schiller *et al.*, 2008; Vishwanatha *et al.*, 2012). To determine which aspects of spine morphogenesis were most affected by the absence of the Sec14 and first four spectrin repeat regions, we quantified the effects of Kal7 and ΔKal7 on synaptic cluster density and location, the association of spines with presynaptic endings, spine length, and spine area; different proteins are known to contribute differently to control of these parameters (Chen *et al.*, 2007; Hotulainen and Hoogenraad, 2010; McMahon and Diaz, 2011).

Dissociated rat neurons were nucleofected with vectors encoding Myc-tagged Kal7 or ΔKal7 at the time of plating and kept in culture for 20 d (DIV20) before fixation and analysis. Exogenous Kalirin was visualized using monoclonal antibody to Myc, and presynaptic endings were identified using antibody to the endogenous vesicular glutamate transporter, Vglut1 (Figure 2). Based on Myc staining, neurons expressing similar levels of the two proteins were compared. Neurons expressing MycΔKal7 extended more MAP2-positive processes than neurons expressing MycKal7, but the processes were shorter (Figure 2, A and B; not quantified). MycKal7 was primarily localized (~70% of total signal) to the tips of dendritic spines (Figure 2, A and C). In agreement with our previous report (Ma *et al.*, 2008b), nearly all MycKal7-positive puncta were apposed to presynaptic Vglut1-positive puncta. In contrast, much of the MycΔKal7 was uniformly distributed throughout the cell soma, and diffuse staining was observed in the dendritic shaft (Figure 2, B and D); ~50% of the MycΔKal7 staining was in spines. Some MycΔKal7-positive clusters along MAP2-positive dendrites were localized at

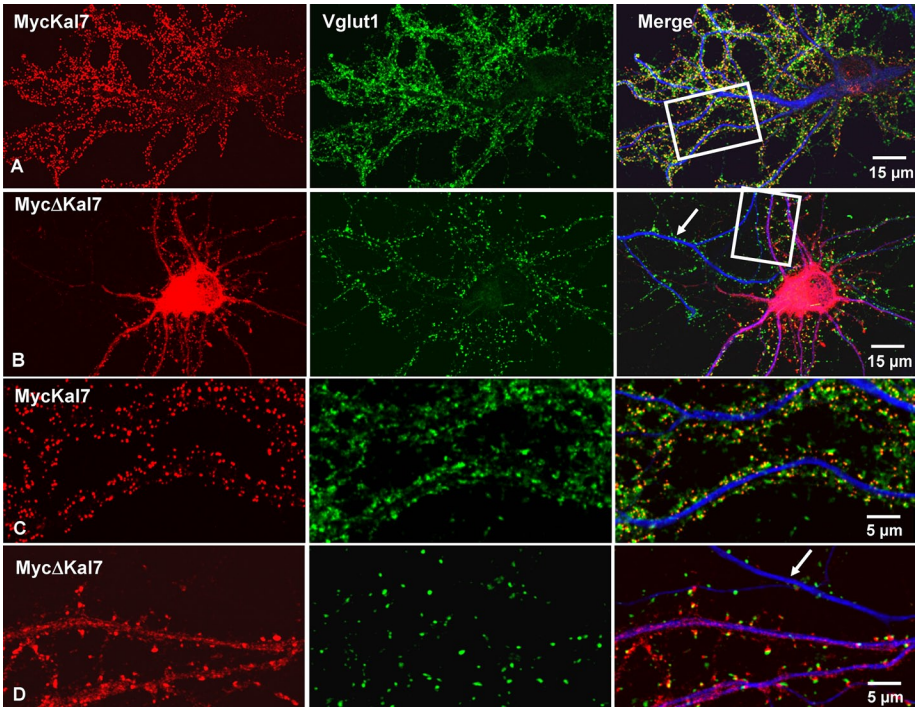

FIGURE 2: MycKal7 and MycΔKal7 differ in their effects on spine and synapse formation. Hippocampal neurons were transfected with vector encoding MycKal7 (A, C) or MycΔKal7 (B, D) at the time of plating (P0). Neurons were fixed at DIV20 for double immunostaining with antibodies to Myc (red), Vglut1 (green: a marker for excitatory presynaptic terminals), and MAP2 (blue: a marker for dendrites). (C) Higher-power image from the boxed dendrites of A. The arrows in B and D show a Myc-negative, nontransfected dendrite. In earlier studies using similar protocols, we established that levels of exogenous MycKal7 were only about double the levels of endogenous Kal7 (Ma *et al.*, 2008b).

the tips of dendritic spines, juxtaposed to Vglut1-positive puncta, but many occurred along the dendritic shaft (Figure 2D).

Synaptic cluster density was determined by counting the number of Myc-positive puncta juxtaposed to Vglut1-positive puncta per unit dendrite length. Both spine and shaft clusters were counted. Synaptic cluster density was threefold higher in neurons expressing MycKal7 than in neurons expressing MycΔKal7 (Figure 3A). We then compared the proportion of total synaptic clusters associated with the dendritic shaft rather than a dendritic spine (Figure 3B). In neurons expressing MycKal7, shaft synapses made up <5% of the total synaptic clusters, whereas >20% of the total synaptic clusters on MycΔKal7-expressing neurons were associated with the shaft. Furthermore, whereas shaft-associated Myc-positive puncta formed by MycKal7 were almost always juxtaposed to a Vglut1-positive punctum, ~20% of the Myc-positive clusters formed by MycΔKal7 on the dendritic shaft lacked a Vglut1-positive presynaptic ending (Figure 3C). Essentially every spine-associated Myc-positive punctum was juxtaposed to a Vglut1-positive punctum (Figure 2, C and D).

Because a Myc/Vglut1-positive cluster defines the juncture of the dendritic spine with its presynaptic ending, the distance (<5 μm) between a Myc/Vglut1-positive cluster and the adjacent dendritic shaft was taken as the measure of spine length (Figure 3D). Neurons expressing MycΔKal7 had slightly shorter spines than neurons expressing MycKal7 (0.79 ± 0.02 vs. 0.95 ± 0.02 μm; $p < 0.01$). The total area encompassed by the synaptic cluster (postsynaptic Myc staining and the adjacent presynaptic Vglut1 staining) was quantified as a measure of synaptic area (Figure 3E). Although the spines formed in neurons expressing MycΔKal7 were shorter, their synaptic cluster areas were substantially larger than in neurons expressing MycKal7 (0.61 ± 0.01 vs. 0.37 ± 0.01 μm^2, respectively; $p < 0.01$).

Taken together, these data indicate that the N-terminal Sec14/spectrin repeat region of Kal7 contributes to synaptic cluster density, location and area, dendritic spine length, and the interaction of presynaptic endings with their postsynaptic targets. We sought to further evaluate the roles of the Sec14/spectrin region by expressing truncated proteins in neurons.

The Sec14 domain of Kalirin plays a role in determining dendritic spine length

To explore the role of the Sec14 domain in neurons, we coexpressed either Kal7 lacking this domain (HA_2ΔSec14Kal7; Figure 4, top) or MycKal7 with green fluorescent protein (GFP) in cortical neurons (Figure 4, A and B). Dendritic spine density was not significantly different in neurons expressing ΔSec14Kal7 and MycKal7 (Figure 4D), and both MycKal7 and ΔSec14Kal7 were largely localized to the tips of dendritic protrusions. However, dendritic spines formed in response to expression of ΔSec14Kal7 were shorter than those formed in response to MycKal7 (Figure 4E); in both cases, most of the protrusions terminated in bulbous heads.

When expressed alone, the Sec14 domain of Kalirin (KalSec14-GFP) was diffusely distributed throughout the soma, dendritic shaft, and dendritic protrusions (Figure 4C). Even when expressed at low levels, expression of KalSec14-GFP had a detrimental effect on neuronal survival; because expression of KalSec14-GFP declined rapidly, cultures nucleofected at the time of plating were fixed on DIV13. The protrusions formed in neurons expressing KalSec14-GFP were less numerous but longer than those present in neurons expressing MycKal7 or ΔSec14Kal7 (Figure 4, C–E). Although not essential for the formation of dendritic spines, our data indicate that the Sec14 domain of Kalirin plays a role in determining protrusion length.

N-terminal fragments of Kal7 stimulate the formation of dendritic spines

Kal4, a minor *Kalrn* splice variant (transcript levels in adult mouse cortex are 5.76 ± 0.17% of that of Kal7), contains only the Sec14 domain and five spectrin repeats (Figure 5, top). Both MycKal4 and MycKalSolo, which contains the Sec14 domain and all nine spectrin repeat regions of Kalirin, lack a GEF domain and PDZ binding motif (Figure 5, top). To evaluate the role of the N-terminal region of Kalirin in spine morphology, we coexpressed these Myc-tagged proteins with GFP in primary rat neurons and fixed them after 18DIV. Like MycKal7, MycKalSolo and MycKal4 were largely localized to puncta at the tips of dendritic protrusions (Figure 5, C and D). In both cases, Myc-positive puncta were closely juxtaposed to presynaptic Vglut1-positive puncta, indicating that the aberrantly shaped protrusions generated in response to expression of MycKalSolo or MycKal4 attracted presynaptic endings (Figure 5, E and F). Of note, the PDZ-binding motif was essential for postsynaptic localization of exogenous Kal7 at earlier

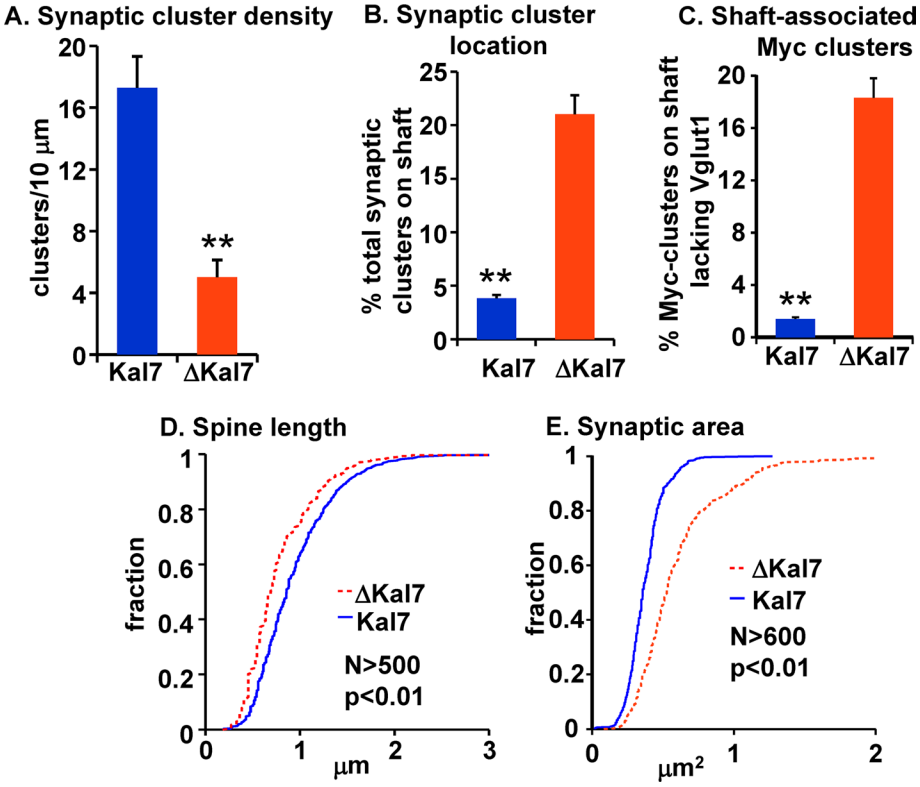

FIGURE 3: Quantification of spine morphology in neurons expressing MycKal7 or MycΔKal7. Hippocampal neurons expressing MycKal7 or MycΔKal7 as described in Figure 2 were analyzed. Myc-positive and Vglut1-positive clusters were manually traced in at least 10 neurons for each group; criteria for inclusion are described in *Materials and Methods*. Myc clusters were identified as spine associated or shaft associated. (A) Juxtaposed or overlapping Myc/Vglut1 clusters on spines or the dendritic shaft are referred to as synaptic clusters; data are reported as clusters/10 µm. Synaptic cluster density was significantly higher in neurons expressing MycKal7 than in neurons expressing MycΔKal7 (17.3 ± 2.0 vs. 5.0 ± 1.1 per 10-µm dendrite; $p < 0.01$; *t* test); error bars show SE of the mean. (B) Myc staining along dendrites within 100 µm of the cell soma was quantified using MetaMorph and identified as spine associated or shaft associated (overlapping the dendritic shaft). Shaft-associated synaptic clusters are plotted as a percentage of total synaptic clusters; shaft-associated synaptic clusters are more common in neurons expressing MycΔKal7 ($p < 0.01$; *t* test). (C) Shaft-associated Myc clusters that lacked an apposed Vglut1 cluster plotted as percentage of total shaft-associated Myc-clusters; this percentage is higher in neurons expressing MycΔKal7 ($p < 0.01$; *t* test). (D) Spine length was significantly longer in neurons expressing MycKal7 than in neurons expressing MycΔKal7 ($p < 0.01$; Kolmogorov–Smirnov). (E) The area occupied by each Myc/Vglut1 cluster was quantified and was significantly smaller in neurons expressing MycKal7 than in neurons expressing MycΔKal7 ($p < 0.01$; Kolmogorov–Smirnov).

developmental time points, when dendritic filopodia predominate (Penzes *et al.*, 2001); endogenous Kal7 and many of the other constituents of mature synapses are not expressed at this stage.

As expected, expression of MycKal7 increased spine formation approximately threefold over the GFP control; in contrast, expression of MycΔKal7 had no effect on spine density (Figure 6A). Expression of MycKal4 or MycKalSolo stimulated the formation of dendritic protrusions, although not to the same extent as the full-length molecule (Figure 6A; $p < 0.05$ for MycKal4 and MycKalSolo vs. GFP).

To quantify differences between the morphology of the protrusions formed in response to expression of MycKalSolo, MycKal4, or MycKal7, we determined synaptic area and spine length as described in Figure 3. Synapses formed in response to MycKal4 were smaller than those formed by the full-length protein (0.45 ± 0.01 vs. 1.04 ± 0.02 µm^2 for Kal7, $p < 0.01$), and synapses formed in response to MycKalSolo were intermediate in size (0.73 ± 0.01 µm^2), larger than Kal4 ($p < 0.01$) and smaller than Kal7 ($p < 0.01$; Figure 6B). The protrusions formed in response to MycKal4 (1.06 ± 0.02 µm) were substantially shorter than those formed in response to MycKalSolo (1.24 ± 0.02 µm, $p < 0.01$), and neither truncated form of Kal7 stimulated the formation of spines that were as long as those formed in response to MycKal7 (1.54 ± 0.02 µm, $p < 0.01$; Figure 6C). Although the morphology of the dendritic protrusions and synaptic clusters formed in response to expression of N-terminal fragments of Kalirin lacking a GEF domain and a PDZ-binding motif was aberrant, the postsynaptic and presynaptic proteins needed to form functional synapses accumulated in or near them. Like full-length Kal7, MycKalSolo and MycKal4 colocalized with the postsynaptic density marker, NR1, as well as with PSD95 and ionotropic glutamate receptor subunit GluR1 at spine tips (PSD95 and GluR1; unpublished data).

Although analytical ultracentrifugation revealed no tendency for the spectrin repeat regions of Kalirin to oligomerize (Vishwanatha *et al.*, 2012), our earlier studies demonstrated interactions between Kal7 and its fifth spectrin repeat, as well as the presence in cortical cytosol of Kal7 in heterogeneous higher–molecular weight complexes (Schiller *et al.*, 2008). To determine whether localization of MycKalSolo and MycKal4 to spine tips required the presence of endogenous Kalirin, we expressed these proteins in cortical neurons prepared from mice lacking all of the isoforms of *Kalrn* (Mandela *et al.*, 2012). In the absence of any endogenous Kalirin proteins, MycKalSolo and MycKal4 still localized to small puncta juxtaposed to Vglut1-positive presynaptic endings (Figure 6, E and F). Difficulty expressing these truncated proteins and maintaining healthy cultures of *Kalrn*-knockout neurons precluded more detailed analysis of morphological differences and synapse formation.

KalSec14 forms an independent domain that interacts with phosphoinositides in a phosphorylation-dependent manner

Because neuronal expression demonstrated a role for the Sec14 domain in Kal7 function, we sought to uncover the underlying mechanism. The tissue-specific use of alternate *Kalrn* promoters appends peptides ranging in length from 5 to 38 amino acids to the N-terminus of the Sec14 domain (McPherson *et al.*, 2004, Mains *et al.*, 2011). A glutathione *S*-transferase (GST)–KalSec14 fusion protein was previously used to demonstrate its lipid-binding abilities (Schiller *et al.*, 2008); to eliminate potential interference from the N-terminal GST tag, we cleaved GST from purified KalSec14 (produced from the A-promoter) and included a short epitope tag on its C-terminus (Figure 7A). Two residues in the Sec14 domain (Thr-79 and Ser-83) can be phosphorylated by protein kinase A, protein kinase C, and CaMKII, and both sites are phosphorylated in Kal7 isolated from mouse striatum (Kiraly *et al.*, 2011, and

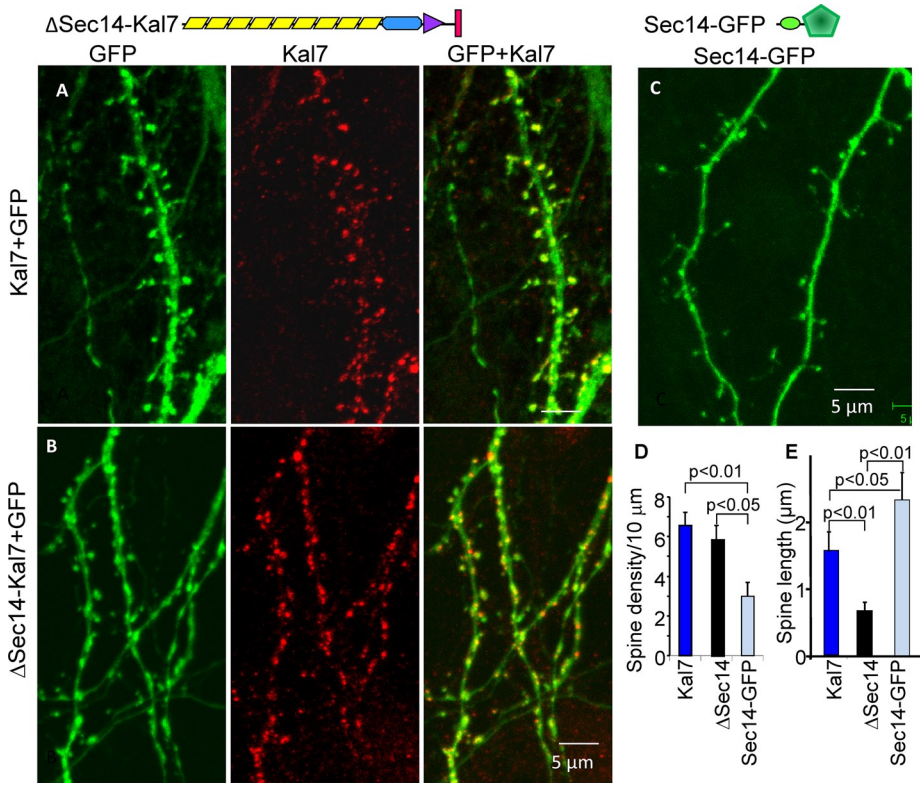

FIGURE 4: The Sec14 domain of Kal7 plays a role in determining spine length. Top, diagrams illustrating the proteins expressed. Hippocampal neurons prepared from P0 rat embryos were doubly transfected with vectors encoding MycKal7 and GFP (A) or HA_2-ΔSec14-Kal7 and GFP (B) or transfected with vector encoding a KalSec14-GFP fusion protein (C) at the time of plating. Neurons were visualized for GFP and Myc (HisMycKal7) or HA (HA_2-ΔSec14-Kal7) (red) at DIV13, a time at which endogenous Kal7 is barely detectable (Ma *et al.*, 2008a). (D) Spine density was indistinguishable in neurons expressing Kal7 and ΔSec14-Kal7 but was significantly lower in Sec14-GFP–expressing neurons (*t* test); synaptic density is lower here than in Figure 3 because synapse formation is not complete in DIV13 neurons. (E) Quantification of spine length revealed that ΔSec14-Kal7 produced significantly shorter spines than MycKal7 ($p < 0.01$), whereas Sec14-GFP produced aberrantly long spines ($p < 0.05$).

unpublished data). Based on the structures of yeast Sec14p and the Sec14 domain of neurofibromin 1, both phosphorylation sites should lie just outside of the putative lipid-binding pocket (Aravind *et al.*, 1999; Mousley *et al.*, 2006). To determine whether phosphorylation of the Sec14 domain of Kalirin at either of these sites might alter its ability to bind lipids, we also purified KalSec14 in which Thr-79 or Ser-83 was mutated to Glu (T79E) or Asp (S83D), respectively, to try to simulate phosphorylation.

The structure of purified KalSec14 was evaluated using circular dichroism. Consistent with its identification as an independent domain, analysis of the spectrum revealed a protein that was 71% α-helix, 19% β-sheet, and 10% unfolded (Figure 7A). We used thermal denaturation to determine whether the isolated KalSec14 domain adopted a stably folded structure (Figure 7B); cooperative unfolding was observed, with a melt temperature of 58 ± 1°C. The KalSec14/T79E protein had similar properties (71% α-helix; thermal melt midpoint, 57 ± 1°C).

We used PIP strips to assess the ability of purified KalSec14, KalSec14/T79E, and KalSec14/S83D to interact with specific lipids. KalSec14 exhibited significant binding to each of the phosphorylated phosphatidylinositides but not to major phospholipids such as phosphatidylethanolamine, phosphatidylcholine, or phosphatidylserine (Figure 7C). KalSec14/T79E and KalSec14/S83D also exhibited a preference for phosphatidylinositides. Compared to the wild-type (WT) protein, KalSec14/T79E showed enhanced binding to each phosphorylated phosphatidylinositide except phosphatidylinositol(3)phosphate (PI(3)P; Figure 7D). Lipid binding by KalSec14/S83D did not differ significantly from that of WT-KalSec14. Taken together, our data suggest that Kal7 interacts with cellular membranes through KalSec14-mediated phosphatidylinositide binding. Furthermore, this interaction may be modulated by the phosphorylation status of KalSec14 and by alterations in cellular phosphatidylinositol phosphate levels. Because the phosphatidylinositides play a crucial role in membrane-trafficking events, we evaluated the effect of KalSec14 expression on receptor-mediated endocytosis using a transferrin uptake assay.

KalSec14 expression reduces transferrin uptake in neuroendocrine cells

Expression of MycKal7, but not MycΔKal7, was previously shown to inhibit transferrin receptor–mediated endocytosis in nonneuronal cells (Schiller *et al.*, 2008), raising the possibility that the inhibition could be due to the Sec14 domain or the first four spectrin repeats. We used a similar system to evaluate the effect of the KalSec14 domain on transferrin endocytosis (Figure 8). We expressed GFP or KalSec14-GFP and assessed uptake of fluorescently tagged transferrin by serum-starved neuroendocrine cells. After a 5-min incubation with fluorescently tagged transferrin (Tf-546), cells were rinsed in serum-free medium and fixed. As in neurons, KalSec14-GFP was diffusely distributed, and expression at high levels or for long periods of time had a deleterious effect on cell morphology. To avoid the disruptive effects of expressing high levels of KalSec14-GFP, less DNA was used in the transfection and the exogenous protein was visualized with GFP antibody. Fluorescence microscopy revealed a significant reduction in Tf-546 internalization in cells expressing KalSec14-GFP when compared with GFP control cells (Figure 8), indicating that exogenous KalSec14 interfered with constitutive membrane trafficking. Whether this effect is directly dependent on the lipid-binding ability of KalSec14 or modulated by phosphorylation remains to be determined.

Kalirin SR4:6 is phosphorylated by Abl1

Our goal was to identify the features unique to the N-terminal portion of Kal7 that make this region important for spine formation, but its tight association with the cytoskeleton and lack of solubility complicated the search for interactors. The *Drosophila* orthologue of *Kalrn*, *dTrio*, was identified in a screen for heterozygous enhancers of lethality caused by mutations in *Abl* (Liebl *et al.*, 2000), and flies with mutations in *dTrio* and *Abl* exhibited similar deficits in axonal growth (Bateman *et al.*, 2000). Extending these observations to vertebrates is difficult, since gene duplication created two dual RhoGEFs, *Kalrn* and *Trio*, both equidistant in sequence from

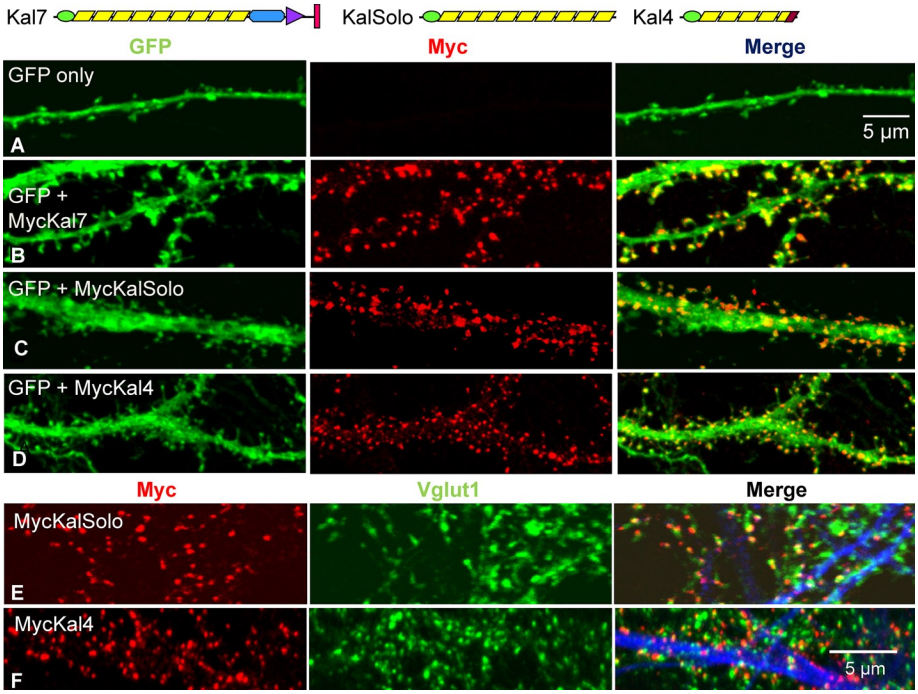

FIGURE 5: Expression of Kalirin constructs lacking the GEF and PDZ-binding domains causes spine formation. Top, diagrams illustrating the proteins expressed. Cortical neurons were transfected with vector encoding GFP only (A) or doubly transfected with vectors encoding GFP and MycKal7 (B), MycΔKal7 (not shown), MycKalSolo (C), or MycKal4 (D) at the time of plating. Neurons were visualized for GFP (green) and Myc (red) at DIV18. Cortical neurons expressing MycKalSolo (E) or MycKal4 (F) were stained simultaneously with antibodies to Myc (red), Vglut1 (green), and MAP2 (blue); for both, most Vglut1 puncta were juxtaposed to Myc puncta.

Drosophila trio (McPherson *et al.*, 2002). In addition, human and other vertebrate genomes encode two *ABL* non–receptor tyrosine kinases, *ABL1* and *ABL2* (Colicelli, 2010; Greuber *et al.*, 2013; Koleske, 2013). Several observations led us to ask whether Kalirin might be phosphorylated by Abl1. First, Kalirin plays an essential role in pathways activated by the PDGFβ receptor (Wu *et al.*, 2013), and PDGFβ receptor engagement in hippocampal neurons activates Abl1 and inhibits NMDA receptor current (Beazely *et al.*, 2008). Second, the spectrin skeleton is believed to form a point of convergence between pathways controlled by Tyr phosphorylation and pathways controlled by intracellular Ca^{2+} (Nedrelow *et al.*, 2003). A phospho-Tyr was identified in SR7 of Kal7 isolated from adult mouse brain, and Tyr residues in SR4 (Tyr-591) and the PDZ-binding motif (Tyr-1653) are phosphorylated in vitro by Fyn, a non–receptor tyrosine kinase (Kiraly *et al.*, 2011).

The purified fragments of Kal7 shown in Figure 9A were incubated with recombinant Abl1 and [^{32}P-γ]ATP for 30 min. Autoradiography after SDS–PAGE revealed preferential phosphorylation of SR4:6 by Abl1 (Figure 9B); no phosphorylation of Sec14:SR1, SR1:3, or the GEF region was detected, and phosphorylation of SR7:9 and GST-Kal7-CT was much less extensive than phosphorylation of SR4:6. Similar experiments using recombinant Abl2 indicated that it does not phosphorylate Sec14:SR1, SR1:3, or SR4:6 (unpublished data).

Tryptic digestion and high-resolution liquid chromatography–tandem mass spectrometry (LC-MS/MS) analysis of recombinant SR4:6 phosphorylated by Abl1 identified two Abl1 phosphorylation sites in SR4—Tyr-591 (Figure 9C) and Tyr-616 (Figure 9D). Tyrosine 591 is also phosphorylated by Fyn, but Abl1, unlike Fyn, does not extensively phosphorylate Tyr-1653, which sits in the PDZ-binding motif of Kal7 and is contained in Kal7-CT (Figure 9B). The extent to which Abl1 phosphorylated Tyr-591 and Tyr-616 under the conditions tested was determined by quantifying all of the peptides that contained the Tyr of interest; based on this analysis, both Tyr-591 and Tyr-616 were extensively phosphorylated (25 and 16%, respectively), whereas no detectable phosphorylation of Tyr-777 or Tyr-838 (both located in SR6) occurred (Figure 9E). Based on the structure predicted for SR7:9 (http://zhanglab.ccmb.med.umich.edu/I-TASSER/), Tyr-591 is located at the interface between helices A and B of SR4, and introduction of a negative charge at this position would be expected to perturb the structure.

Abl1 phosphorylation of KalSR4:6 increases calpain-mediated proteolysis

Both the formation of new spines and the remodeling of existing spines require changes in the existing cytoskeleton; endoproteolytic cleavage of cytoskeletal proteins is known to contribute to this process. Calcium-mediated activation of μ-calpain and ERK-mediated activation of m-calpain are known to contribute to this remodeling process (Wu and Lynch, 2006; Zadran *et al.*, 2009; Baudry *et al.*, 2013; Chamma *et al.*, 2013). KalSR4:6 was previously shown to contain a trypsin-sensitive site in the B-C loop of SR5 (AR^{722}/DS; Figure 9E; Vishwanatha *et al.*, 2012). We tested the hypothesis that phosphorylation of KalSR4:6 by Abl1 alters its sensitivity to calpain-mediated proteolysis in vitro. KalSR4:6 that had been incubated with [γ-^{32}P]ATP and Abl1 and KalSR4:6 incubated under the same conditions but without Abl1 were exposed to increasing concentrations of μ-calpain. SDS–PAGE revealed that ^{32}P-labeled KalSR4:6 phosphorylated by Abl1 (Figure 10A, left) was more sensitive to μ-calpain–mediated degradation than the nonphosphorylated protein (Figure 10A, right). The only predicted calpain cleavage site in KalSR4:6 (PS^{714}/LG) is located in the same loop that contains the previously identified trypsin-sensitive site (Vishwanatha *et al.*, 2012).

We next asked whether KalSR4:6 in which Tyr-591 or Tyr-616 had been replaced by a negatively charged amino acid (Glu) exhibited a similar increase in calpain sensitivity. SDS–PAGE analysis of purified KalSR4:6/Y^{591}E and KalSR4:6/Y^{616}E revealed that each migrated more slowly than KalSR4:6, suggesting a major effect of each point mutation on the properties of the protein, even during SDS–PAGE (Figure 10B, left). Consistent with this conclusion, KalSR4:6/Y591/E was more sensitive to calpain-mediated degradation than the wild-type protein, with nearly complete degradation after incubation with 50 ng of calpain (Figure 10B, right). Mutation of Tyr-616 to Glu had a lesser effect on sensitivity to μ-calpain (Figure 10B, right). Preferential Abl1-mediated phosphorylation of Tyr-591 versus Tyr-616 and a more powerful effect of Tyr-591 phosphorylation on sensitivity to calpain cleavage were confirmed by analyzing the stability of Abl1-phosphorylated KalSR4:6/Y591E and KalSR4:6/Y616E (unpublished data).

Inhibition of Abl alters spine morphology

The role of the BCR/ABL fusion protein in cancer led to the development of compounds that inhibit ABL1/ABL2 without affecting

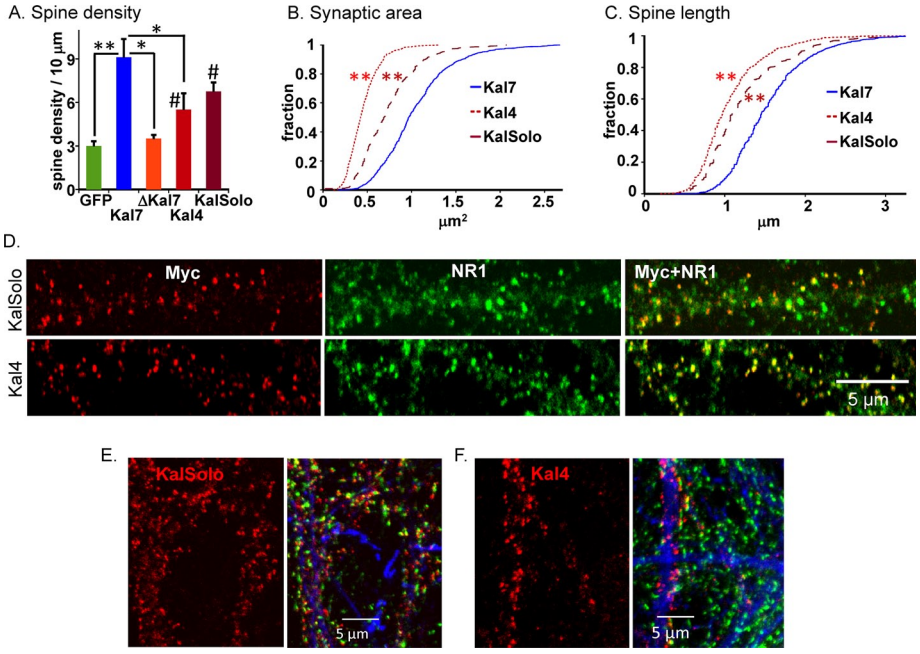

FIGURE 6: Neurons expressing MycKalSolo or MycKal4 form spines with aberrant morphology. (A) Spine-like protrusions along dendrites (at least 10 neurons in each group) within 100 µm of the cell soma were quantified using MetaMorph as described; one-way analysis of variance followed by Dunnett's test; *$p < 0.05$, **$p < 0.01$, #$p < 0.05$, compared with GFP and ΔKal7. MycΔKal7 did not differ from GFP in its ability to induce spine formation. Myc-positive and Vglut1-positive clusters on the dendritic shaft were included in the measurements for hippocampal neurons reported in Figure 3; for the cortical neurons shown here, Myc-positive clusters on the dendritic shaft were excluded. Synaptic (Myc/Vglut1 cluster) area (B) and spine length (C) were quantified using MetaMorph; data are displayed as a Kolmogorov–Smirnov distribution. (B) Kal7 larger than KalSolo and KalSolo larger than Kal4 (all **$p < 0.01$, Kolmogorov–Smirnov). (C) Kal7 larger than KalSolo and KalSolo larger than Kal4 (all **$p < 0.01$, Kolmogorov–Smirnov). (D) DIV20 cortical neurons expressing MycKalSolo or MycKal4 (as described in Figure 5) were stained simultaneously with antibodies to Myc (red) and NR1 (green); antibody specific to MAP2 was included to verify the identity of dendrites (not shown). Antisera to PSD95 and GluR1 produced staining patterns similar to those shown for NR1 (data not shown). (E, F) Cortical neurons prepared from E20 total Kalirin-knockout embryos were nucleofected with vectors encoding MycKal7 (not shown), MycKalSolo, or MycKal4; Myc (red), Vglut1 (green), and MAP2 (blue) were visualized simultaneously in cultures fixed on DIV19. As observed in primary neurons from wild-type rats, MycKalSolo and MycKal4 localized to spine-like structures; Vglut1-positive endings were juxtaposed to the small puncta formed by MycKalSolo and MycKal4.

other non–receptor tyrosine kinases (Colicelli, 2010; Greuber *et al.*, 2013). We exposed DIV18 cortical neurons prepared from wild-type mice to one of these inhibitors (GNF-5) for 6 h and then quantified dendritic protrusion density and length; membrane-targeted farnesylated GFP (fGFP) was expressed to facilitate the analysis (Figure 10C). Drug-treated and control neurons were fixed and stained for GFP and filamentous actin. The density of actin-rich dendritic protrusions on the dendrites of wild-type cortical neurons increased significantly after GNF-5 treatment, with no effect on protrusion length (Figure 10C). Based on its effects on KalSR4:6, phosphorylation of Kal7 by Abl1 may target it for cleavage by calpain. If so, inhibition of Abl1 would be expected to stabilize Kal7; the ability of Kal7 to stimulate the formation of dendritic spines could account for the observed increase in protrusion density.

We next asked whether cultures prepared from Kal7^{KO} cortices responded differently to GNF-5 treatment (Figure 10D). When DIV18 cortical neurons from Kal7^{KO} mice were exposed to the same level of GNF-5, protrusion density was unaffected. Although GNF-5 was without effect on dendritic protrusion length in wild-type neurons, Kal7^{KO} neurons responded to drug treatment with an increase in protrusion length (Figure 10D). The fact that GNF-5 had distinctly different effects on the dendritic protrusions formed by wild-type and Kal7^{KO} neurons is consistent with the conclusion that Kal7 plays an important role in Abl-mediated effects on spine morphology. The ability of Kal7 to promote spine maturation (Ma *et al.*, 2008a) may limit the formation of long, filopodia-like protrusions; lacking this maturation factor, the protrusions formed by Kal7^{KO} neurons may be more likely to elongate.

DISCUSSION

Spine morphology, a key determinant of excitatory synaptic transmission, is regulated by the actin cytoskeleton (Bloodgood and Sabatini, 2005; Araya *et al.*, 2006; Hotulainen and Hoogenraad, 2010; McMahon and Diaz, 2011; Nestor *et al.*, 2011; Yuste, 2013). The Sec14 and first four spectrin repeats of Kal7 contribute to control of synaptic cluster area and location, transsynaptic communication, spine density, and spine length. Long-term potentiation in hippocampal slice preparations and control of spine head size and spine formation by cortical neurons in response to ephrinB require the GEF activity of Kal7 (Penzes *et al.*, 2003; Lemtiri-Chlieh *et al.*, 2011), but spine formation does not. The ability of the Sec14 and spectrin repeat regions of Kalirin to modulate spine formation and size provides sites at which diverse signaling pathways can regulate these processes.

The Sec14 domain of Kal7 and spine length

Kal7 lacking only its Sec14 domain (ΔSec14Kal7; Figure 4, diagram) produced the normal number of spines, but the spines were short. Consistent with this, expression of the isolated Sec14 domain increased spine length without increasing spine formation. Sec14 domains occur in only ~20 murine proteins (Mousley *et al.*, 2006; Gupta *et al.*, 2012); some bind small, hydrophobic ligands, whereas others interact with small GTPases and their GEFs and GAPs. The Sec14 domains of Mcf2 and Mcf2l are involved in intramolecular interactions and bind phosphoinositides (Ueda *et al.*, 2004; Ishikawa *et al.*, 2005; Kostenko *et al.*, 2005). The ability of similar lipid-binding proteins to move lipids between membranes is suited to a role in changing cell morphology (Maeda *et al.*, 2013).

Both GST-KalSec14 and KalSec14-rhodopsin bound multiple phosphatidylinositides and not the more prevalent phospholipids. Threonine 79, predicted by homology modeling to be in an α-helix that stabilizes the lipid-binding pocket, can be phosphorylated by multiple synaptic protein kinases and is phosphorylated in vivo (Kiraly *et al.*, 2011). Its replacement with a phosphomimetic mutation enhanced Sec14 binding to most of the phosphatidylinositides. Although different phosphatidylinositides are localized to different

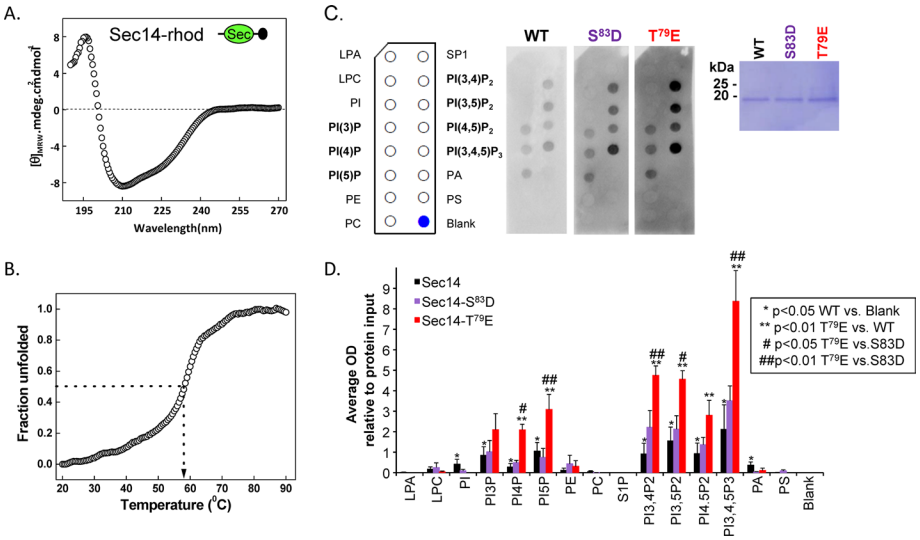

FIGURE 7: The Sec14 domain of Kalirin interacts with phosphoinositides. (A) The circular dichroism spectrum (average of six determinations) of purified rhodopsin-tagged KalSec14 (inset illustrates location of epitope tag [black circle]) was evaluated from 190 to 270 nm; the spectrum obtained for KalSec14/T79E was indistinguishable (not shown). (B) Cooperative unfolding was observed in a thermal denaturation study of KalSec14; the transition temperature observed was 58 ± 1°C for WT-KalSec14 and 57 ± 1°C for KalSec14/T79E. (C) Purified WT-KalSec14, KalSec14/T79E, and KalSec14/S83D (1 µg/ml; inset: Coomassie-stained membrane demonstrating the purity of the recombinant proteins) were incubated with PIP strips as described in *Materials and Methods*; bound protein was visualized using antibody to the rhodopsin epitope tag. The lipids on the PIP strips are identified. (D) Data from five experiments were quantified; after background subtraction and normalization to the binding of WT-KalSec14 to $PI(3,4,5)P_3$, data were averaged; error bars represent SE of the mean. No significant binding was observed to lysophosphatidic acid (LPA), lysophosphatidylcholine (LPC), phosphatidylethanolamine (PE), phosphatidylcholine (PC), sphingosine-1-phosphate (SP1), or phosphatidylserine (PS). WT-Sec14 exhibited significant binding to each of the phosphatidylinositides (*$p < 0.05$ WT vs. blank; Holm–Sidak multiple-comparisons test). Compared to WT-Sec14 and Sec14/S83D, Sec14/T79E exhibited enhanced binding to each phosphorylated phosphatidylinositide except PI(3)P (**,##$p < 0.01$ Sec14/T^{79}E vs. WT and Sec14/S^{83}D, respectively; Holm–Sidak multiple-comparisons test). After background subtraction and averaging, data for Sec14/S83D did not differ significantly from WT.

When expressed in fibroblasts, Kal7, but not ΔKal7, blocked the uptake of transferrin (Schiller *et al.*, 2008); the transferrin/transferrin receptor complex is bound by the AP2 complex and internalized in a clathrin-mediated process (Abe *et al.*, 2008). Expression of KalSec14-GFP diminished transferrin uptake, linking Kalirin to membrane trafficking. Internalization of transferrin by its receptor is blocked when plasma membrane levels of phosphatidylinositol 4,5-bisphosphate are rapidly reduced (Abe *et al.*, 2008). The diminished levels of NR2B on the surface of $Kal7^{KO}$ neurons could reflect the role of the Kal7 Sec14 domain in membrane trafficking. α-Amino-3-hydroxy-5-methyl-4-isoxazolepropionic acid receptor clustering at the PSD is affected by phosphatidylinositides (Arendt *et al.*, 2010), and phosphoinositide-3-kinase activation affects spine and synapse formation (Cuesto *et al.*, 2011).

Spine length is decreased by repeated stimulation of cultured neurons with NMDA or by blocking γ-aminobutyric acid type A receptors and increased by short-term treatment with tetrodotoxin (Segal, 1995; Papa and Segal, 1996). Loss of SynCAM 1, a synaptic adhesion molecule (Cheadle and Biederer, 2012), and ablation of PSD95 (Beique *et al.*, 2006) increase spine length. Overexpression of the actin-binding domain of α–actinin-2, which binds NMDA receptor subunits NR1 and NR2B (Wyszynski *et al.*, 1997), increases spine length without altering spine density.

compartments, KalSec14-GFP was diffusely distributed when expressed in neurons or in neuroendocrine cells, and prolonged or high-level expression was toxic.

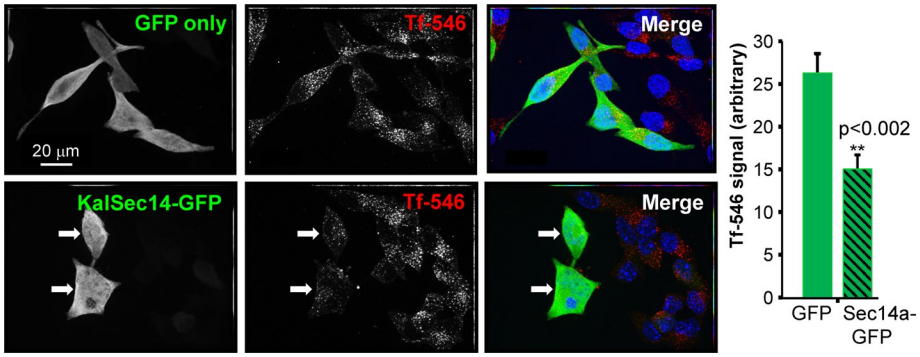

FIGURE 8: KalSec14-GFP disrupts receptor-mediated endocytosis in AtT-20 corticotrope tumor cells. (Left) Magnified 63× images showing Alexa Fluor 546–transferrin uptake (red) by AtT-20 corticotrope tumor cells expressing either GFP (top) or KalSec14-GFP (bottom). Cells were exposed to Alexa Fluor 546–Tf for 5 min at ~24 h after transfection and were then fixed, stained, and imaged. Scale bars, 20 µm. (Right) Quantification of internalized 546-Tf. Data were collected using MetaMorph; values were normalized to cell size and relative to GFP control cells ($n = 8$ for GFP and 12 for Sec14-GFP; error bars, ± SEM; **$p < 0.002$). Results were confirmed in an independent experiment.

The spectrin repeats of Kal7, Abl, and spine formation

Unlike ΔKal7, which did not increase spine formation, expression of ΔSec14Kal7 (Figure 1A, diagram) increased spine density as much as Kal7. Fragments of Kal7 composed only of SRs were often insoluble, so we examined proteins that included the N-terminal Sec14 domain and four (Kal4) or nine (KalSolo) SRs. Their effects on spine density, length, and area were graded. Although the spines that formed in response to Kal4 and KalSolo were shorter, with smaller synaptic areas than spines formed in response to Kal7, postsynaptic markers (PSD-95, GluR1, NR1) accumulated at their tips, and presynaptic endings were juxtaposed.

Overexpression of α–actinin-2, with its SRs and PDZ-binding motif, increases both spine length and density (Nakagawa *et al.*, 2004). Hippocampal neurons deficient in Septin7 have abnormally long spines (Xie *et al.*, 2007). Septin7 forms a complex with ERK3 and MK5 and is localized at the spine base. Of interest, the SR region of Kalirin interacts with MK5, which phosphorylates a

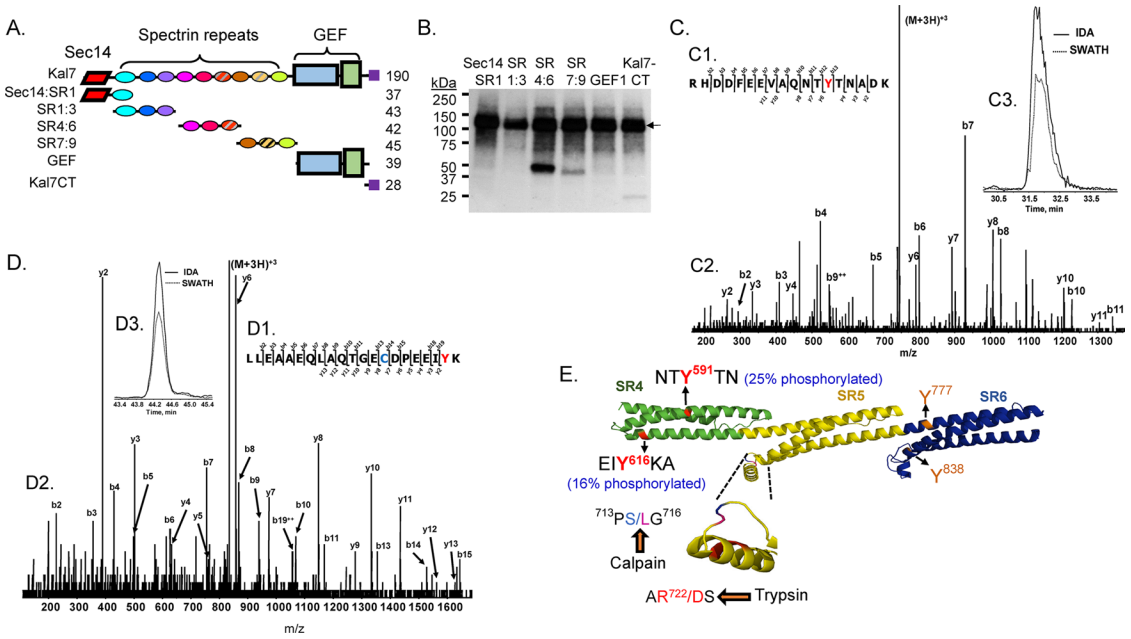

FIGURE 9: Phosphorylation of Kal SR4:6 by Abl1. (A) The purified fragments of Kalirin (0.5 μM) shown in the diagram were each exposed to recombinant Abl1 (10 nM) along with 5 μM ATP and 0.75 μCi [^{32}P-γ]ATP at 32°C for 30 min. (B) The reactions were stopped by boiling each sample into Laemmli sample buffer; after SDS–PAGE and transfer to a polyvinylidene fluoride membrane, phosphorylated proteins were visualized by autoradiography (3-h exposure). In addition to autophosphorylated Abl1 (135 kDa; arrow), KalSR4:6 was phosphorylated (band at ~50 kDa); less extensive phosphorylation of KalSR7:9 and Kal7-CT was also detectable. (C, D) The reaction was scaled up as described in *Materials and Methods*, and phosphorylated SR4:6 recovered from a silver-stained 4–15% acrylamide gel was subjected to in-gel digestion with trypsin, followed by LC-MS/MS identification of phosphorylated Tyr residues. Sites are identified using the NP_114451.2 numbering scheme for *Kalrn*. MS/MS fragmentation patterns for the Tyr-591 (C) and Tyr-616 (D) peptides are shown. Manual verification and the site of Tyr modification (red Y) are illustrated in C1 and D1. The b- and y-ion series peak assignments are shown (C2, D2). Extracted ion chromatograms of the parent ion $(M+2H)^{2+}$ for the IDA and SWATH runs were retention time aligned (C3 and D3). Note that the Cys (blue) in the Tyr-616 peptide was acrylamide gel modified (propionamide). (E) Model illustrates the location of the four Tyr residues in KalSR4:6. For each Tyr, percentage phosphotyrosine (shown in parentheses) was calculated relative to the sum of all of the peptides containing that Tyr residue (phosphorylated or not). The protease-sensitive insert in the B-C loop of SR5 (inset) contains the only predicted calpain-cleavage site (Vishwanatha *et al.*, 2012)

Ser in the SH3-binding motif in SR3 (Brand *et al.*, 2012), perhaps contributing to the effects of Kalirin on spine length.

The molecular basis underlying the genetic association of *dTrio* and *dAbl* has not been clarified (Bateman *et al.*, 2000; Liebl *et al.*, 2000; Lin and Greenberg, 2000). *Abl1* and *Abl2/Arg*, mammalian homologues of *dAbl*, are both expressed in neurons (Perez de Arce *et al.*, 2010; Greuber *et al.*, 2013; Koleske, 2013). Abl proteins localize to sites of actin remodeling, and multiple receptor tyrosine kinases interact with and are phosphorylated by Abl (Colicelli, 2010). We focused on Abl1 because it phosphorylated a site in SR4, but SR7:9 was phosphorylated by Abl2. Like Kal7, Abl1 localizes to the PSD, where it phosphorylates PSD-95 (Beazely *et al.*, 2008; Perez de Arce *et al.*, 2010; Greuber *et al.*, 2013). Activation of Abl can be triggered by receptor tyrosine kinases, chemokine receptors, oxidative stress, and interactions with regulatory proteins (Greuber *et al.*, 2013). Abl1 phosphorylates two Tyr residues (Tyr-591 and Tyr-616) in the fourth SR of Kalirin; Kal7 isolated from mouse brain is phosphorylated on Tyr-591 (Kiraly *et al.*, 2011).

Phosphorylation of Tyr-591 produced a substantial change in the conformation and protease sensitivity of KalSR4:6. Controlled proteolysis plays an essential role in long-term potentiation (Baudry *et al.*, 2013) and spine morphogenesis (Lynch *et al.*, 2006; Wu and Lynch, 2006; Amini *et al.*, 2013). Specifically, calpain inhibitors block LTP in vitro and in vivo (Amini *et al.*, 2013). Phosphorylation of a single Tyr in αII-spectrin reduces its susceptibility to calpain-mediated proteolysis (Nicolas *et al.*, 2002; Siminovic *et al.*, 2006). In contrast, phosphorylation of KalSR4:6 by Abl1 increased its sensitivity to calpain cleavage. The site phosphorylated by Abl1 is conserved in Kalirin and Trio. Although well-conserved in Kalirin, the protease-sensitive loop in KalSR4:6 is not present in Trio. Phosphorylation of Kal7 at Tyr-591 could also affect its localization or its ability to interact with other proteins. The third SR of Kalirin contains an SH3-binding motif, raising the possibility that it could interact with the SH3 domain of Abl1. The interaction of Abl1 with F-actin and G-actin (Colicelli, 2010) could then contribute to the ability of Kal4 and Kal-Solo, which lack a GEF domain, to increase spine formation.

Highly selective inhibitors of Abl1/Abl2 were developed to treat chronic myeloid leukemia (Colicelli, 2010; Greuber *et al.*, 2013). We were able to demonstrate an increase in the density of dendritic protrusions 6 h after the addition of GNF-5 to primary cultures of cortical neurons. Of note, because GNF-5 inhibits Abl1 and Abl2 (both of which are expressed in these neurons), both Abl1 and Abl2 may contribute to the observed changes in protrusion density. To our knowledge, this is the first time the neuronal effects of this class of Abl inhibitors have been evaluated. The fact that protrusion density was not increased when Kal7^{KO} neurons were exposed to GNF-5 establishes a role for Kal7 in the response. Stabilization of Kal7 in response to inhibition of Abl1 phosphorylation of Tyr-591 and/or

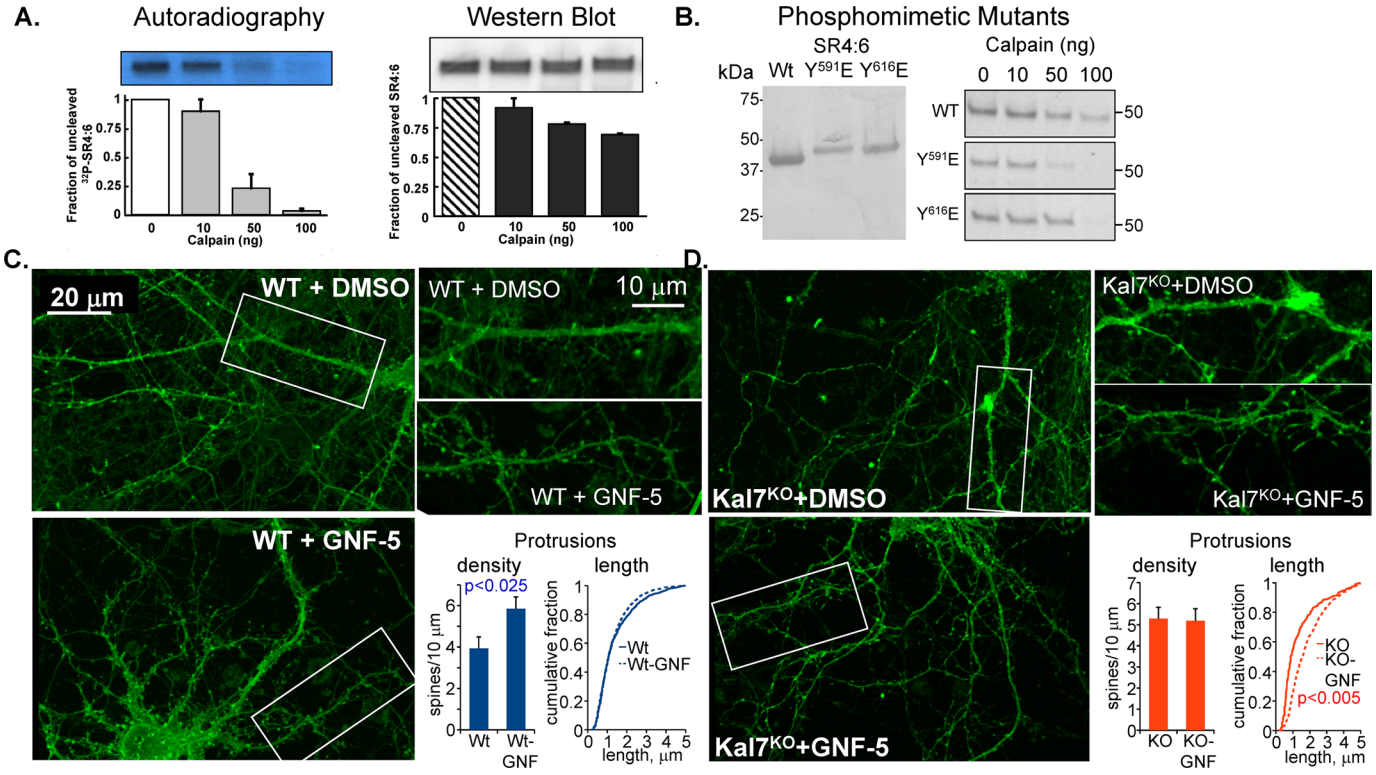

FIGURE 10: Phosphorylation of KalSR4:6 by Abl1 increases its sensitivity to calpain. (A) KalSR4:6 phosphorylated with [γ-^{32}P]ATP by Abl1 or exposed to the same conditions in the absence of ATP and Abl1 was exposed to the indicated amount of μ-calpain for 60 min at 37°C. Digested samples were fractionated by SDS–PAGE and transferred to polyvinylidene fluoride (PVDF) membranes; ^{32}P-labeled KalSR4:6 was visualized by autoradiography (left), and unlabeled KalSR4:6 was visualized by Western blot (right) using an antibody to SR4:7 (JH2580; Penzes *et al.*, 2000). The amount of intact KalSR4:6 remaining was quantified; error bars show range of duplicate experiments. (B) Purified recombinant KalSR4:6 and KalSR4:6 with a phosphomimetic mutation at position 591 (SR4:6/Y591E) or 616 (SR4:6/Y616E) was fractionated by SDS–PAGE, transferred to a PVDF membrane, and visualized with Coomassie brilliant blue; mutation of either Tyr residue altered the mobility of the protein during electrophoresis. The purified proteins (1 μg each) were exposed to the indicated dose of μ-calpain as described. The reaction was stopped, and the SDS–PAGE fractionated products were visualized with Coomassie; mutation of either site increased the calpain sensitivity of the protein. (C, D) DIV18 cortical neurons from WT (C) and Kal7^{KO} (D) mice were exposed to medium containing 10 μM GNF-5 in DMSO, or an equivalent volume of DMSO, for 6 h and fixed. Images obtained using an Axiovert 200M with Apotome for optical sectioning were coded and scored by a blinded observer. GNF-5 increased the dendritic protrusion density in WT but not Kal7^{KO} neurons (C) while increasing the protrusion length in Kal7^{KO} but not WT neurons (D). N = 9–14 WT neurons and 6–8 Kal7^{KO} neurons; N = 1187–1652 WT protrusions and 306–838 Kal7^{KO} protrusions.

Tyr-616 could contribute to the observed increase in protrusion density.

MATERIALS AND METHODS

Primary neuronal cultures and transfection

Cultures were prepared from postnatal day 0 (P0; cortical or hippocampal) Sprague–Dawley rats or embryonic day 20 (E20; cortical) KalSR$^{KO/KO}$ mice as described (Ma *et al.*, 2003, 2008a). In KalSR$^{KO/KO}$ mice, elimination of exon 13 in the spectrin repeat region ablates production of all major isoforms of Kalirin (Mandela *et al.*, 2012). Freshly dissociated neurons ([1–2] × 10^6 neurons) were nucleofected using program O-003 (Amaxa, Cologne, Germany) with the vectors to be described. Nucleofected neurons were kept in Neurobasal A (embryonic) or Neurobasal (P0) maintenance medium for up to 3 wk as described (Ma *et al.*, 2011). The vectors encoding HisMycKal7, HisMycΔKal7, HisMycKalSolo, HisMycKal4, HA$_2$ΔSec14Kal7 (starts EEWIELRL-), and KalSec14-GFP (ends -LDYNH; Schiller *et al.*, 2008) and fGFP (Francone *et al.*, 2010) were described. The pGEX6P1-KalSec14 vectors included the rhodopsin epitope (italicized) at the COOH terminus (M^{1}VLSG–LRLSL^{172}*GATETSQVAPA*; Kalirin numbering: AAF66018.1, GI:7650388).

Immunocytochemistry

Immunostaining of cultures was performed as described (Ma *et al.*, 2008b). Neurons were fixed with 4% paraformaldehyde in phosphate-buffered saline (PBS). After permeabilization with 0.20% Triton X-100 in blocking buffer (1% bovine serum albumin [BSA], 5% normal goat and/or donkey serum in PBS, pH 7.4), followed by incubation for 50 min in blocking buffer at room temperature, cells were doubly or triply stained with appropriate primary antibodies overnight at 4°C. Primary antibodies were visualized with appropriate secondary antibodies: Cy3-donkey anti-mouse, fluorescein isothiocyanate (FITC)–donkey anti-rabbit, FITC-donkey anti-rat, and FITC-donkey anti-guinea pig immunoglobulin G (IgG) were from Jackson ImmunoResearch Laboratories (West Grove, PA); Alexa Fluor 633–goat anti-rabbit and anti-mouse IgG were from Molecular Probes (Eugene, OR). Images were obtained using a Zeiss (Jena, Germany) LSM510 confocal microscope. Hoechst nuclear stain (Invitrogen, Grand Island,

NY) and tetramethylrhodamine isothiocyanate (TRITC)–phalloidin (Sigma-Aldrich, St. Louis, MO) were used where indicated.

Antibodies

Rabbit antibodies to the following antigens were used: Kal7 (affinity-purified JH2958, 1:200; Penzes *et al.*, 2000), MAP2 (1:500, AB5622; Millipore, Billerica, MA), and Myc (1:100, #39688; Abcam, Cambridge, MA). Mouse monoclonal antibodies to the following antigens were used: PSD95 (clone 28/43, 1:300; NeuroMab Facility, University of California, Davis, Davis, CA), NR1 (1:300, #556308; BD PharMingen, San Diego, CA), MAP2 (1:500, #1406; Sigma-Aldrich), and Myc (9E10, 1:20). Guinea pig antibody to Vglut1 (1:3000, AB5909; Millipore) and rat antibody to GFP (1:1000; Nacalai Tesque, Kyoto, Japan) were used where indicated.

GNF-5 treatment

Sparsely plated WT or Kal7$^{KO/KO}$ cortical neurons were nucleofected with vector encoding fGFP at plating and grown on coverslips for 18 d. On DIV18, neuronal maintenance medium was removed entirely and replaced with maintenance medium containing 10 μM GNF-5 (diluted from a 10 mM stock in dimethyl sulfoxide [DMSO]; Sigma-Aldrich) or control (1 μl/ml DMSO; Colicelli, 2010; Greuber *et al.*, 2013). Plates were returned to the incubator for 6 h, and cells were then fixed with 4% paraformaldehyde in PBS. Cultures were stained for GFP using a rat primary antibody and FITC-labeled secondary antibody and for filamentous actin using TRITC-phalloidin (Sigma-Aldrich).

Transferrin uptake

AtT-20 corticotropic tumor cells plated on glass coverslips in four-well dishes were transfected 24 h later with vectors encoding EGFP or KalSec14-GFP. At 24 h after transfection, cells were serum starved for 30 min and then incubated with 0.25 mg/ml Alexa Fluor 546–tagged transferrin (Tf; Invitrogen) in serum-free medium for 5 min at 37°C/5% CO_2. Cells were then quickly rinsed with serum-free medium and immediately fixed with 4% paraformaldehyde in PBS. Coverslips were stained using the GFP antibody and Hoechst (Invitrogen) nuclear stain.

Image analysis and quantification

Spine density and synaptic clusters were quantified by a blinded observer after the scale bar for the image was calibrated using MetaMorph (Molecular Devices, Sunnyvale, CA) as described (Ma *et al.*, 2008a). Briefly, for initial quantification of spine density and synaptic clusters (Figures 2–6), a stack of images (*Z* step, 0.3 μm) was acquired using a 63× objective (2.5 digital zoom factor), and dendrites were visualized in three dimensions using the Zeiss LSM Image Browser. Synaptic clusters were manually traced using MetaMorph. Spine density and synaptic clusters were counted, and cluster size was measured after images were calibrated and thresholds were set to ensure that all interesting structures were included in the analysis. Quantifications were performed using MetaMorph and were limited to dendrites within 100 μm of the soma. The length of each traced spine was measured using MetaMorph. Data are presented as average ± SEM. The effects of MycΔKal7, MycKalSolo, and MycKal4 were compared with those of GFP and MycKal7; comparisons were made among neurons displaying similar levels of Myc signal.

For analysis of transferrin uptake by AtT-20 cells and of the effects of GNF-5 on neuronal morphology, images were taken using an Axiovert 200M epifluorescence microscope and a 63× oil objective and ApoTome for optical sectioning. Image processing was done using AxioVision software, with identical settings within experiments. Images used for analysis were compressed *Z*-stack series. For each image, *Z*-steps were taken through the entire depth of the cell population within each frame. The *Z*-step distance ranged from 0.49 to 0.62 μm for Tf uptake experiments and from 0.32 to 0.48 μm for GNF-5 treatment experiments. To measure Tf uptake, MetaMorph was used to trace individual cells and determine average 546-Tf (red) signal. Intensity values were averaged within groups and then compared. Images from GNF-5–treated neurons were coded and analyzed by a blind observer. For each neuron, dendritic protrusions within 100 μm of the cell soma and <5 μm in length were counted, and protrusion density/10 μm of dendrite was calculated. Protrusion length was determined by measuring the distance between the point where the protrusion met the shaft and the tip of the protrusion. After all data were collected, images were decoded, and data were averaged within groups.

Preparation and analysis of Sec14-rhodopsin

A pGEX-6P vector encoding the Sec14 domain of rat Kalirin (M^{1}VLSG–LRLSL^{172}*GATETSQVAPA*) with a rhodopsin epitope tag at the C-terminus (*TETSQVAPA*; Liu and Krieger, 2002) was constructed and verified by sequence analysis (sites are identified using the U88157.1 numbering scheme for *Kalrn*). Protein expression and purification were carried out essentially as described (Vishwanatha *et al.*, 2012). Briefly, the GST-fusion protein from a 500-ml culture was bound to a 5-ml GSTrap-4B column (GE Healthcare, Piscataway, NJ), eluted by overnight cleavage with GST-HRV3C protease (GenWay Biotech, San Diego, CA), and purified by chromatography on a Q-Sepharose column (5 mm × 40 mm) equilibrated with 20 mM NaTES, pH 8.0, at a flow rate of 0.5 ml/min. Proteins were eluted with a linear gradient to 500 mM NaCl in the same buffer over 180 min. The purity of the KalSec14-rhodopsin was >93% as assessed by staining with Coomassie brilliant blue R250. pGEX-6P vectors encoding two phosphomimetic mutants of KalSec14-rhodopsin were constructed; Thr-79 was mutated to Glu (Sec14/T79E), and Ser-83 was mutated to Asp (Sec14/S83D). Vector sequences were verified, and mutant proteins were purified in a similar manner. Protein concentrations were determined by measuring absorbance at 280 nm (using the molar extinction coefficient calculated from tryptophan and tyrosine content). A Jasco J-715 spectropolarimeter with a thermostated cell housing was used as described (Vishwanatha *et al.*, 2012); spectra were recorded between 190 and 270 nm. Secondary structure analyses were carried out using CDSSTR (Sreerama and Woody, 2003) with the reference database available in DICHROWEB (http://dichroweb.cryst.bbk.ac.uk/html/home.shtml). Thermal unfolding profiles were determined by raising the temperature from 20 to 90°C at a rate of 1°C/min.

Lipid binding

PIP strips (P-6001; Echelon Biosciences, Salt Lake City, UT) were blocked with 3% fatty acid–free BSA (A6003; Sigma-Aldrich) in Tris-buffered saline containing 0.1% Tween-20 (TTBS) for 1 h at room temperature and then incubated with 1 μg/ml purified Sec14 protein (wild type or mutant) diluted in blocking solution for 1 h at room temperature. PIP strips were washed three times in TTBS and visualized using a mouse monoclonal antibody to the rhodopsin tag and a horseradish peroxidase–conjugated anti-mouse secondary antibody. Signals were quantified using a GeneGnome digital imaging system and identical exposure times. After background subtraction, densitometric data for all three proteins were normalized to the signal obtained for wild-type Sec14 binding to PI(3,4,5)P_3, its preferred interactor. Across experiments, normalized values

were averaged within groups and represented as relative values ± SEM. Note that in earlier PIP-strip binding studies (Schiller *et al.*, 2008) GST was not removed from the N-terminus of the Sec14 domain (M^{1}VLSG–LLSRL^{186}).

Abl1 phosphorylation of KalSR4:6

Purified KalSR4:6 (1.0 µM in a final volume of 25 µl) was incubated with recombinant mouse Abl1 (100 nM) and 2 mM ATP for 1 h at 32°C, as recommended by the supplier (SignalChem, Richmond, Canada). Denatured samples were loaded onto a 4–15% acrylamide gel (Bio-Rad, Hercules, CA) and visualized using the SilverSNAP stain (Pierce, Rockford, IL); control KalSR4:6 (no Abl1) and Abl1 phosphorylated KalSR4:6 were excised, destained, and subjected to in-gel tryptic digestion (V51111; Promega, Madison, WI) at the Yale/NIDA Neuroproteomics Center (New Haven, CT). Peptides extracted with 80% acetonitrile/0.1% trifluoroacetic acid were dried under vacuum, dissolved in 70% formic acid, and immediately diluted with 50 mM potassium phosphate buffer at 25°C. Information-dependent acquisition (IDA) and SWATH acquisitions were carried out on an AB SCIEX Triple TOF 5600 coupled with a Waters (Milford, MA) nanoACQUITY UPLC system. Digests (5 µl) were loaded onto a Waters Symmetry C18 180 µm × 20 mm trap and separated on a nanoACQUITY 1.7 um BEH300 C18 (75 µm × 150 mm) column. Peptide separations were performed at 500 nl/min with buffer A (0.1% formic acid) and buffer B (CH_3CN containing 0.1% formic acid). A linear gradient (70 min) was run with 1% buffer B at initial conditions, 35% buffer B at 70 min, 95% buffer B at 70.33 min, and column re-equilibration for 20 min. IDA runs were carried out at high sensitivity with resolution ~16–18K in the MS/MS (maximum of 30 MS/MS per cycle) at 0.05 s/scan and time-of-flight MS scan of 0.25 s. SWATH acquisition was carried out over the mass range of 400–1250 with setting at 26-Da scan window with 1-Da overlap (i.e., 400–425, 424–450, etc.) for a total of 34 SWATH windows/cycle. Acquired LC-MS/MS data were analyzed using Analyst (version 2.5) and PeakView (version 2.0; AB SCIEX). Protein identification and site modification assignment used MASCOT (Matrix Science, Boston, MA) searches; modification sites of interest were manually verified. Skyline (MacLean *et al.*, 2010) was used to obtain precursor ion quantitation from SWATH data on the various modification sites. Peak intensities for all peptides containing the site of interest (phosphorylated or not) were summed and used to calculate percentage tyrosine phosphorylation. Sites were identified using the NP_114451.2 numbering scheme for *Kalrn*.

Sensitivity to cleavage by calpain I (Sigma-Aldrich) was tested using KalSR4:6 phosphorylated by Abl1, as well as purified KalSR4:6, KalSR4:6/Y^{591}E, and KalSR4:6/Y^{616}E. For preparation of radiolabeled KalSR4:6, recombinant protein (0.5 µM in a final volume of 25 µl) was incubated with Abl1 (10 nM), 5 µM ATP, and 0.75 µCi/ml [^{32}P]ATP as described. The entire reaction mixture was then incubated with varying doses of calpain in 25 mM sodium 3-(N-morpholino)propanesulfonic acid, pH 7.2, containing 1 µM $CaCl_2$ for 60 min at 37°C. After SDS–PAGE and transfer to a polyvinylidene fluoride membrane, radiolabeled products were identified by autoradiography; unlabeled proteins were identified by Western blot analysis using an antibody to SR4:6 (JH2580).

Statistical analyses

Analyses were performed with Student's *t* test or JMP6 software (SAS Institute, Cary, NC) using one-way analysis of variance (ANOVA), followed by Dunnett's test to assess statistical significance between groups; $*p < 0.05$ or $**p < 0.01$ was considered statistically significant. The lipid-binding data were compared using two-way ANOVA with repeated measures for the four sets of measurements (Holm–Sidak multiple-comparisons test; Prism [GraphPad, La Jolla, CA] or SigmaPlot [Systat, San Jose, CA]).

ACKNOWLEDGMENTS

This work was supported by grants from the National Institutes of Health (DK-32948, DA-15464, DA-23082, and P30 DA018343) and by support from the Scoville Endowment and the Janice and Rodney Reynolds Endowment. We thank Darlene D'Amato for incomparable technical assistance, Laura Urbanski for assistance with the calpain studies, Kathrin Wilczak and Mary LoPresti for assistance with sample preparation, Lisa Chung for help with pTyr quantitation, and Prashant Mandela for assistance with the KalSR^{KO} mice.

REFERENCES

Abe N, Inoue T, Galvez T, Klein L, Meyer T (2008). Dissecting the role of PtdIns(4,5)P_2 in endocytosis and recycling of the transferrin receptor. J Cell Sci 121, 1488–1494.

Alam MR, Caldwell BD, Johnson RC, Darlington DN, Mains RE, Eipper BA (1996). Novel proteins that interact with the COOH-terminal cytosolic routing determinants of an integral membrane peptide-processing enzyme. J Biol Chem 271, 28636–28640.

Amini M *et al.* (2013). Conditional disruption of calpain in the CNS alters dendrite morphology, impairs LTP, and promotes neuronal survival following injury. J Neurosci 33, 5772–5784.

Aravind L, Neuwald AF, Ponting CP (1999). Sec14p-like domains in NF1 and Dbl-like proteins indicate lipid regulation of Ras and Rho signaling. Curr Biol 9, 195–197.

Araya R, Jiang J, Eisenthal KB, Yuste R (2006). The spine neck filters membrane potentials. Proc Natl Acad Sci USA 103, 17961–17966.

Arendt KL, Rovo M, Fernandez-Monreal M, Knafo S, Petrok CN, Martens JR, Esteban JA (2010). PIP3 controls synaptic function by maintaining AMPA receptor clustering at the postsynaptic membrane. Nat Neurosci 13, 36–44.

Bateman J, Shu H, Van Vactor D (2000). The guanine nucleotide exchange factor trio mediates axonal development in the *Drosophila* embryo. Neuron 26, 93–106.

Baudry M, Chou MM, Bi X (2013). Targeting calpain in synaptic plasticity. Expert Opin Ther Targets 17, 579–592.

Beazely MA, Weerapura M, MacDonald JKF (2008). Abelson tyrosine kinase links PDGFbeta receptor activation to cytoskeletal regulation of NMDA receptors in CA1 hippocampal neurons. Mol Brain 1, 20.

Beique JC, Lin DT, Kang MG, Aizawa H, Takamiya K, Huganir RL (2006). Synapse-specific regulation of AMPA receptor function by PSD-95. Proc Natl Acad Sci USA 103, 19535–19540.

Bloodgood BL, Sabatini BL (2005). Neuronal activity regulates diffusion across the neck of dendritic spines. Science 310, 866–869.

Brand F, Schumacher S, Kant S, Menon MB, Simon R, Turgeon B, Britsch S, Meloche S, Gaestel M, Kotlyarov A (2012). The extracellular signal-regulated kinase 3 (mitogen-activated protein kinase 6 [MAPK6])-MAPK-activated protein kinase 5 signaling complex regulates septin function and dendrite morphology. Mol Cell Biol 32, 2467–2478.

Cahill ME, Jones KA, Rafalovich I, Xie Z, Barros CS, Muller U, Penzes P (2012). Control of interneuron dendritic growth through NRG1/erbB4-mediated kalirin-7 disinhibition. Mol Psychiatry 17, 199–107.

Chamma I, Heubl M, Chevy Q, Renner M, Moutkine I, Eugene E, Poncer JC, Levi S (2013). Activity-dependent regulation of the K/Cl transporter KCC2 membrane diffusion, clustering, and function in hippocampal neurons. J Neurosci 33, 15488–15503.

Cheadle L, Biederer T (2012). The novel synaptogenic protein Farp1 links postsynaptic cytoskeletal dynamics and transsynaptic organization. J Cell Biol 199, 985–1001.

Chen LY, Rex CS, Casale MS, Gall CM, Lynch G (2007). Changes in synaptic morphology accompany actin signaling during LTP. J Neurosci 27, 5363–5372.

Colicelli J (2010). ABL tyrosine kinases: evolution of function, regulation, and specificity. Sci Signal 3, re6.

Colomer V, Engelender S, Sharp AH, Duan K, Cooper JK, Lanahan A, Lyford G, Worley P, Ross CA (1997). Huntingtin-associated protein 1 (HAP1) binds to a Trio-like polypeptide, with a rac1 guanine nucleotide exchange factor domain. Hum Mol Genet 6, 1519–1525.

Cuesto G, Enriquez-Barreto L, Carames C, Cantarero M, Gasull X, Sandi C, Ferrus A, Acebes A, Morales M (2011). Phosphoinositide-3-kinase activation controls synaptogenesis and spinogenesis in hippocampal neurons. J Neurosci 31, 2721–2733.

Debant A, Serra-Pages C, Seipel K, O'Brien S, Tang M, Park S-H, Streuli M (1996). The multidomain protein Trio binds the LAR transmembrane tyrosine phosphatase, contains a protein kinase domain, and has separate rac-specific and rho-specific guanine nucleotide exchange factor domains. Proc Natl Acad Sci USA 93, 5466–5471.

Francone VP, Ifrim MF, Rajagopal C, Leddy CJ, Wang Y, Carson JH, Mains RE, Eipper BA (2010). Signaling from the secretory granule to the nucleus: Uhmk1 and PAM. Mol Endocrinol 24, 1543–1558.

Giorgi M, Cianci CD, Gallagher PG, Morrow JS (2006). Spectrin oligomerization is cooperatively coupled to membrane assembly: a linkage targeted by many hereditary hemolytic anemias? Exp Mol Pathol 70, 215–230.

Greuber EK, Smith-Pearson P, Wang J, Pendergast AM (2013). Role of ABL family kinases in cancer: from leukaemia to solid tumours. Nat Rev Cancer 13, 559–571.

Gupta AB, Wee LE, Zhou YT, Hortsch M, Low BC (2012). Cross-species analyses identify the BNIP-2 and Cdc42GAP homology (BCH) domain as a distinct functional subclass of the CRAL_TRIO/Sec14 superfamily. PLoS One 7, e33863.

Hayashi-Takagi A *et al*. (2010). Disrupted-in-Schizophrenia 1 (DISC1) regulates spines of the glutamate synapse via Rac1. Nat Neurosci 13, 327–332.

Hotulainen P, Hoogenraad CC (2010). Actin in dendritic spines: connecting dynamics to function. J Cell Biol 189, 619–629.

Ipsaro JJ, Mondragon A (2010). Structural basis for spectrin recognition by ankyrin. Blood 115, 4093–4101.

Ishikawa K *et al*. (2005). An autosomal dominant cerebellar ataxia linked to chromosome 16q22.1 is associated with a single nucleotide substitution in the 5′ untranslated region of the gene encoding a protein with spectrin repeat and rho guanine-nucleotide exchange-factor domains. Am J Hum Genet 77, 280–296.

Jones KA, Srivastava DP, Allen JA, Strachan RT, Roth BL, Penzes P (2009). Rapid modulation of spine morphology by the 5-HT2A serotonin receptor through kalirin-7 signaling. Proc Natl Acad Sci USA 106, 19575–19580.

Kiraly DD, Stone KL, Colangelo CM, Abbott T, Wang Y, Mains RE, Eipper BA (2011). Identification of kalirin-7 as a potential post-synaptic density signaling hub. J Proteome Res 10, 2828–2841.

Koleske AJ (2013). Molecular mechanisms of dendrite stability. Nat Rev Neurosci 14, 536–550.

Koo TH, Eipper BA, Donaldson JG (2007). Arf6 recruits the Rac GEF Kalirin to the plasma membrane facilitating Rac activation. BMC Cell Biol 8, 29.

Kostenko EV, Mahon GM, Cheng L, Whitehead IP (2005). The Sec14 homology domain regulates the cellular distribution and transforming activity of the Rho-specific guanine nucleotide exchange factor Dbs. J Biol Chem 280, 2807–2817.

Krug T, Manso H, Gouvela L, Sobral J, Xavier JM, Oliveira SA (2010). Kalirin: a novel genetic risk factor for ischemic stroke. Hum Genet 127, 513–523.

Kushima I *et al*. (2012). Resequencing and association analysis of the KALRN and EPHB1 genes and their contribution to schizophrenia susceptibility. Schizophr Bull 38, 552–560.

Lemtiri-Chlieh F, Zhao L, Kiraly DD, Eipper BA, Mains RE, Levine ES (2011). Kalirin-7 is necessary for normal NMDA receptor-dependent synaptic plasticity. BMC Neurosci 12, 126.

Lesch KP *et al*. (2008). Molecular genetics of adult ADHD: converging evidence from genome-wide association and extended pedigree linkage studies. J Neural Transm 115, 1573–1585.

Liebl EC, Forsthoefel DJ, Franco LS, Sample SH, Hess JE, Cowger JA, Chandler MP, Shupert AJ, Seeger MA (2000). Dosage-sensitive, reciprocal genetic interactions between the Abl tyrosine kinase and the putative GEF trio reveal trio's role in axon pathfinding. Neuron 26, 107–118.

Lin MZ, Greenberg ME (2000). Orchestral maneuvers in the axon: trio and the control of axon guidance. Cell 101, 239–242.

Liu B, Krieger M (2002). Highly purified scavenger receptor class B, type I reconstituted into phosphtidylcholine/cholesterol liposomes mediates high affinity high density lipoprotein binding and selective lipid uptake. J Biol Chem 277, 34125–34135.

Lynch G, Rex CS, Gall CM (2006). LTP consolidation: substrates, explanatory power, and functional significance. Neuropharmacology 52, 12–23.

Ma XM, Huang JP, Kim EJ, Zhu Q, Kuchel GA, Mains RE, Eipper BA (2011). Kalirin-7, an important component of excitatory synapses, is regulated by estradiol in hippocampal neurons. Hippocampus 21, 661–677.

Ma XM, Huang J, Wang Y, Eipper BA, Mains RE (2003). Kalirin, a multifunctional Rho guanine nucleotide exchange factor, is necessary for maintenance of hippocampal pyramidal neuron dendrites and dendritic spines. J Neurosci 23, 10593–10603.

Ma XM, Kiraly DD, Gaier ED, Wang, Kim EJ, Levine ES, Eipper BA, Mains RE (2008a). Kalirin-7 is required for synaptic structure and function. J Neurosci 28, 12368–12382.

Ma XM, Wang Y, Ferraro F, Mains RE, Eipper BA (2008b). Kalirin-7 is an essential component of both shaft and spine excitatory synapses in hippocampal interneurons. J Neurosci 28, 711–724.

MacLean B, Tomazela DM, Shulman N, Chambers M, Finney GL, Frewen B, Kern R, Tabb DL, Liebler DC, MacCoss MJ (2010). Skyline: an open source document editor for creating and analyzing targeted proteomics experiments. Bioinformatics 26, 966–968.

Maeda K, Anand K, Chiapparino A, Kumar A, Poletto M, Kaksonen M, Gavin A-C (2013). Interactome map uncovers phosphatidylserine transport by oxysterol-binding proteins. Nature 501, 257–261.

Mains RE, Kiraly DD, Eipper-Mains JE, Ma X-M, Eipper BA (2011). *Kalrn* promoter usage and isoform expression respond to chronic cocaine exposure. BMC Neurosci 12, 20.

Mandela P, Yankova M, Conti LH, Ma XM, Grady J, Eipper BA, Mains RE (2012). Kalrn plays key roles within and outside of the nervous system. BMC Neurosci 13, 136.

McMahon SA, Diaz E (2011). Mechanisms of excitatory synapse maturation by trans-synaptic organizing complexes. Curr Op Neurobiol 21, 221–227.

McPherson CE, Eipper BA, Mains RE (2002). Genomic organization and differential expression of Kalirin isoforms. Gene 284, 41–50.

McPherson CE, Eipper BA, Mains RE (2004). Kalirin expression is regulated by multiple promoters. J Mol Neurosci 22, 51–62.

McPherson CE, Eipper BA, Mains RE (2005). Multiple novel isoforms of Trio are expressed in the developing rat brain. Gene 347, 125–135.

Mousley CJ, Tyeryar KR, Ryan MM, Bankaitis VA (2006). Sec14p-like proteins regulate phosphoinositide homeostasis and intracellular protein and lipid trafficking in yeast. Biochem Soc Trans 34, 346–350.

Murray PS *et al*. (2012). beta-Amyloid 42/40 ratio and kalirin expression in Alzheimer disease with psychosis. Neurobiol Aging 33, 2807–2816.

Nakagawa T, Engler JA, Sheng M (2004). The dynamic turnover and functional roles of a-actinin in dendritic spines. Neuropharmacology 47, 734–745.

Nedrelow JH, Cianci CD, Morrow JS (2003). c-Src binds aII spectrin's Src homology 3 (SH3) domain and blocks calpain susceptibility by phosphorylating Tyr^{1176}. J Biol Chem 278, 7735–7741.

Nestor MW, Cai X, Stone MR, Block RJ, Thompson SM (2011). The actin binding domain of b1-spectrin regulates the morphological and functional dynamics of dendritic spines. PLOS 6, e16197.

Nicolas G *et al*. (2002). Tyrosine phosphorylation regulates alphaII spectrin cleavage by calpain. Mol Biol Cell 22, 3527–3536.

Papa M, Segal M (1996). Morphological plasticity in dendritic spines of cultured hippocampal neurons. Neuroscience 71, 1005–1011.

Penzes P, Beeser A, Chernoff J, Schiller MR, Eipper BA, Mains RE, Huganir RL (2003). Rapid induction of dendritic spine morphogenesis by trans-synaptic ephrinB-EphB receptor activation of the Rho-GEF kalirin. Neuron 37, 263–274.

Penzes P, Johnson RC, Alam MR, Kambampati V, Mains RE, Eipper BA (2000). An Isoform of Kalirin, a brain-specific GDP-GTP exchange factor, is enriched in the post-synaptic density fraction. J Biol Chem 275, 6395–6403.

Penzes P, Johnson RC, Sattler R, Zhang X, Huganir RL, Kambampati V, Mains RE, Eipper BA (2001). The neuronal Rho-GEF Kalirin-7 interacts with PDZ domain-containing proteins and regulates dendritic morphogenesis. Neuron 29, 229–242.

Perez de Arce K, Varela-Nallar L, Farias O, Cifuentes A, Bull P, Couch BA, Koleske AJ, Inestrosa NC, Alvarez AR (2010). Synaptic clustering of PSD-95 is regulated by c-Abl through tyrosine phosphorylation. J Neurosci 30, 3728–3738.

Ratovitski EA *et al*. (1999). Kalirin inhibition of inducible nitric-oxide synthase. J Biol Chem 274, 993–999.

Saito K, Tautz L, Mustelin T (2007). The lipid-binding SEC14 domain. Biochim Biophys Acta 1771, 719–726.

Schaaf G *et al*. (2008). Functional anatomy of phospholipid binding and regulation of phosphoinositide homeostasis by proteins of the Sec14 superfamily. Mol Cell 29, 191–206.

Schiller MR, Ferraro F, Wang Y, Ma XM, McPherson CE, Sobota JA, Schiller NI, Mains RE, Eipper BA (2008). Autonomous functions for the Sec14p/spectrin-repeat region of Kalirin. Exp Cell Res 314, 2674–2691.
Segal M (1995). Morphological alterations in dendritic spines of rat hippocampal neurons exposed to N-methyl-D-aspartate. Neurosci Lett 193, 73–76.
Sheetz MP, Sable JE, Dobereiner H-G (2006). Continuous membrane-cytoskeleton adhesion requires continuous accommodation to lipid and cytoskeleton dynamics. Annu Rev Biophys Biomol Struct 35, 417–434.
Siminovic M, Zhang Z, Cianci CD, Steitz TA, Morrow JS (2006). Structure of the calmodulin alphaII-spectrin complex provides insight into the regulation of cell plasticity. J Biol Chem 281, 34333–34340.
Sreerama N, Woody RW (2003). Structural composition of betaI- and betaII-proteins. Protein Sci 12, 384–388.
Ueda S, Kataoka T, Satoh T (2004). Role of the Sec14-like domain of Dbl family exchange factors in the regulation of Rho family GTPases in different subcellular sites. Cell Signal 16, 899–906.
van Rijssel J, van Buul JD (2012). The many faces of the guanine-nucleotide exchange factor trio. Cell Adh Migr 6, 482–487.
Vishwanatha KS, Wang Y, Keutmann HT, Mains RE, Eipper BA (2012). Structural organization of the nine spectrin repeats of kalirin. Biochemistry 51, 5663–5673.
Wang L *et al*. (2007). Peakwide mapping on chromosome 3q13 identifies the kalirin gene as a novel candidate gene for coronary artery disease. Am J Hum Genet 80, 650–663.
Wu H-Y, Lynch DR (2006). Calpain and synaptic function. Mol Neurobiol 33, 215–236.
Wu JH, Fanaroff AC, Sharma KC, Smith LS, Brian L, Eipper BA, Mains RE, Freedman NJ, Zhang L (2013). Kalirin promotes neointimal hyperplasia by activating Rac in smooth muscle cells. Arterioscler Thromb Vasc Biol 33, 702–708.
Wyszynski M, Lin J, Rao A, Nigh E, Beggs AH, Craig AM, Sheng M (1997). Competitive binding of a-actinin and calmodulin to the NMDA receptor. Nature 385, 438–442.
Xie Z, Photawala H, Cahill ME, Srivastava DP, Woolfrey KM, Shum CY, Huganir RL, Penzes P (2008). Coordination of synaptic adhesion with dendritic spine remodeling by AF-6 and kalirin-7. J Neurosci 28, 6079–6091.
Xie Y, Vessey JP, Konecna A, Dahm R, Macchi P, Kiebler MA (2007). The GTP-binding protein septin 7 is critical for dendrite branching and dendritic-spine morphology. Curr Biol 17, 1746–1751.
Youn H, Jeoung M, Koo Y, Ji H, Markesbery WR, Ji I, Ji TH (2007). Kalirin is under-expressed in Alzheimer's disease hippocampus. J Alzheimers Dis 11, 385–397.
Yuste R (2013). Electrical compartmentalization in dendritic spines. Annu Rev Neurosci 36, 429–449.
Zadran S, Jourdi H, Rostamiani K, Qin Q, Bi X, Baudry M (2009). Brain-derived neurotrophic factor and epidermal growth factor activate neuronal m-calpain via mitogen-activated protein kinase-dependent phosphorylation. J Neurosci 30, 1086–1095.